

THESIS FOR THE DEGREE OF DOCTOR OF PHILOSOPHY

**Synthesis and properties of π -conjugated polymers for
organic photovoltaics**

RENEE KROON



Polymer Technology
Department of Chemical and Biological Engineering
CHALMERS UNIVERSITY OF TECHNOLOGY
Göteborg, Sweden 2013

SYNTHESIS AND PROPERTIES OF π -CONJUGATED POLYMERS FOR ORGANIC PHOTOVOLTAICS

RENEE KROON

© RENEE KROON, 2013.

ISBN 978-91-7385-801-4

Doktorsavhandlingar vid Chalmers tekniska högskola

Ny serie nr 3482

ISSN 0346-718X

Polymer Technology

Department of Chemical and Biological Engineering

Chalmers University of Technology

SE-412 96 Gothenburg

Sweden

Telephone + 46 (0) 31-772 10 00

Cover: Chalmers Solar, the platform for solar research at Chalmers. The logo was constructed by illuminating ($\lambda = 365$ nm) two emissive polymers, PFPA (blue light-emission) and a poly(phthalimide-alt-thiophene) (orange light-emission). Photo by Agnes Stepan, Tim Steckler, Liona Samplonius and Renee Kroon.

Chalmers Reproservice

Gothenburg, Sweden 2013

Synthesis and properties of π -conjugated polymers for organic photovoltaics

RENEE KROON

Department of Chemical and Biological Engineering

Chalmers University of Technology

Gothenburg, Sweden

ABSTRACT

Organic photovoltaics is a renewable energy technology able to solve global warming and the upcoming energy gap, issues that both originate from fossil fuel consumption. Out of all renewable energy sources, the Sun is the only source that produces enough energy to fulfill all our energy needs, now and in the future. Photovoltaics based on π -conjugated polymers are envisioned to offer a low cost alternative to the present technology, but optimization of the polymer structure is needed to achieve efficiencies high enough to make this technology economically viable.

This thesis deals with both the optimization of several parent structures via the process of energy level engineering and establishing structure-property relationships upon alteration of these parent structures. The initial work explored the effect of carbon-silicon exchange on various physical, optical and photovoltaic properties of fluorene/silafluorene-based copolymers. The optical, redox and photovoltaic properties of these polymers remained virtually unchanged except for the thermal behavior. The work was continued by optimizing the energy levels and bandgap of TQ1 with the aim to surpass its already high power conversion efficiency of 6%. Aside from improved spectral coverage and energy level optimization, several interesting structure-property relationships were found. Finally, another well-performing structure, PDPPTPT, was modified with alkoxy sidechains to investigate the effect on various polymer properties. Aside from a redshifted absorption, polymer properties were altered suggesting additional flexibility in the polymer backbone. By comparing polymer and oligomer properties, methoxy substitution seems to initially increase melting and crystallization temperatures, but this trend is then supposedly counteracted due to increased irregularity in the polymer backbone.

Keywords: *Conjugated polymers, organic photovoltaics, energy level engineering, structure-property relationships*

LIST OF PUBLICATIONS

This thesis is partially based on the following scientific papers, referred to by their Roman numerals in the text. The papers are appended at the end of the thesis.

- Paper I.** **New quinoxaline and pyridopyrazine-based polymers for solution processable photovoltaics**
Renee Kroon, Robert Gehlhaar, Timothy T. Steckler, Patrik Henriksson, Christian Müller, Jonas Bergqvist, Afshin Hadipour, Paul Heremans, Mats R. Andersson
Solar Energy Materials and Solar Cells, 2012, 105, 280–286
- Paper II.** **Effect of electron-withdrawing side chain modifications on the optical properties of thiophene-quinoxaline acceptor based polymers**
Renee Kroon, Angelica Lundin, Camilla Lindqvist, Patrik Henriksson, Timothy Steckler, Mats R. Andersson
Accepted for publication, Polymer, 2013, XXX,XXX-XXX
- Paper III.** **Blue-to-transmissive of solution processable donor-acceptor polymers**
Stefan Hellström, Patrik Henriksson, Renee Kroon, Ergang Wang and Mats R. Andersson
Organic Electronics, 2011, 12, 1406-1413
- Paper IV.** **The influence of alkoxy substitutions on the properties of diketopyrrolopyrrole-phenyl copolymers**
Z. George, R. Kroon, R. Gehlhaar, G. Gbabode, A. Lundin, S. Hellström, C. Müller, Y. Geerts, P. Heremans, M. R. Andersson
Manuscript
- Paper V.** **Charge separation dynamics in a narrow gap polymer-PbS nanocrystal blend for efficient hybrid solar cells**
Claudia Piliago, Marianna Manca, Renee Kroon, Maksym Yarema, Krisztina Szendrei, Mats R. Andersson, Wolfgang Heiss and Maria A. Loi
Journal of Materials Chemistry, 2012, 22, 24411-24416

CONTRIBUTION REPORT

- Paper I.** Synthesis and chemical, physical and optical characterization of all polymers and organic intermediates. Interpretation of most results and writing the manuscript with input from the co-authors.
- Paper II.** Synthesis and chemical, physical and optical characterization of all polymers and organic intermediates. Interpretation of most results and writing the manuscript with input from the co-authors.
- Paper III.** Responsible for the synthesis and chemical, physical and optical characterization of TQ2 and all its organic intermediates, some writing.
- Paper IV.** Synthesis of PDPPTPT, oligomers and the associated organic intermediates. Most of the physical and optical characterization. Responsible for part of the interpretation of the results and partly writing the manuscript with input from the co-authors.
- Paper V.** Synthesis and characterization of PDPPTPT

PUBLICATIONS NOT INCLUDED IN THE THESIS

- Paper VI.** **Interlayer for modified cathode in highly efficient ITO-free organic solar cells**
Zheng Tang, L. Matthias Andersson, Zandra George, Koen Vandewal, Kristofer Tvingstedt, Patrik Henriksson, Renee Kroon, Mats R. Andersson, Olle Inganäs
Advanced Materials, 2012, 24, 554-558

TABLE OF CONTENTS

INTRODUCTION.....	1
1.1 <i>WORLD ENERGY PRODUCTION.....</i>	1
1.2 <i>RENEWABLE ENERGY SOURCES.....</i>	2
1.3 <i>ECONOMICAL VIABILITY.....</i>	2
1.4 <i>THE SOLAR SPECTRUM.....</i>	3
1.5 <i>SILICON SOLAR CELLS.....</i>	4
1.6 <i>POLYMER SOLAR CELLS.....</i>	4
1.7 <i>AIM OF THE THESIS.....</i>	6
ORGANIC SOLAR CELLS.....	7
2.1 <i>BANDGAP AND EXCITATIONS.....</i>	7
2.2 <i>CHARGE GENERATION IN ORGANIC SEMICONDUCTORS.....</i>	8
2.3 <i>ARCHITECTURE OF ORGANIC SOLAR CELLS AND PERFORMANCE PARAMETERS.....</i>	11
2.4 <i>DESIGNING MATERIALS FOR ORGANIC SOLAR CELLS.....</i>	13
2.5 <i>OUTLINE.....</i>	18
SILAFLUORENE-BASED COPOLYMERS.....	21
3.1 <i>INTRODUCTION.....</i>	21
3.2 <i>SYNTHESIS.....</i>	22
3.3 <i>PHYSICAL AND OPTO-ELECTRONIC PROPERTIES.....</i>	23
3.4 <i>PHOTOVOLTAIC PERFORMANCE.....</i>	25
TQ1 DERIVATIVES.....	27
4.1 <i>INTRODUCTION.....</i>	27
4.2 <i>ACCEPTOR MODIFICATIONS ON TQ1.....</i>	27
4.2.1 <i>Synthesis.....</i>	28
4.2.2 <i>Physical and optical properties.....</i>	29
4.2.3 <i>Photovoltaic performance.....</i>	31
4.3 <i>SIDE CHAIN MODIFICATIONS ON TQ1.....</i>	33
4.3.1 <i>Synthesis.....</i>	33
4.3.2 <i>Physical and optical properties.....</i>	34
4.4 <i>OTHER TQ1 RELATED POLYMERS.....</i>	36
4.4.1 <i>Synthesis.....</i>	36
4.4.2 <i>Physical and optical properties.....</i>	38
4.4.3 <i>Photovoltaic performance.....</i>	39
4.5 <i>TQ1 DERIVATIVES IN ELECTROCHROMICS.....</i>	40
4.5.1 <i>Physical and opto-electronic properties.....</i>	40
DIKETOPYRROLOPYRROLE-BASED POLYMERS.....	43
5.1 <i>INTRODUCTION.....</i>	43
5.2 <i>SYNTHESIS.....</i>	44
5.3 <i>PHYSICAL AND OPTICAL PROPERTIES.....</i>	45
5.4 <i>PHOTOVOLTAIC PERFORMANCE.....</i>	46
5.5 <i>PDPPTPT AS DONOR POLYMER IN HYBRID SOLAR CELLS.....</i>	47
CONCLUDING REMARKS.....	49
ACKNOWLEDGEMENTS.....	50
REFERENCES.....	52

Chapter 1

INTRODUCTION

1.1 World energy production

The exchange of wood and biofuels for coal as an energy source initiated the industrial age, around 1750. Since then, the world got accustomed to power generated from fossil fuels and at present, the world power consumption amounts to ~16 TW globally. Around 87% of the consumed power is generated via fossil fuels which include oil, coal and natural gas, while the source for the remaining 13% is hydroelectric, nuclear and renewable energy (Fig. 1.1a). Considering only what energy sources are converted to supply the total electrical power, coal is by far the most used fossil fuel before natural gas and oil (Fig. 1.1b).^[1, 2] Fossil fuels are available, reliable and energy dense and therefore a cheap energy source.

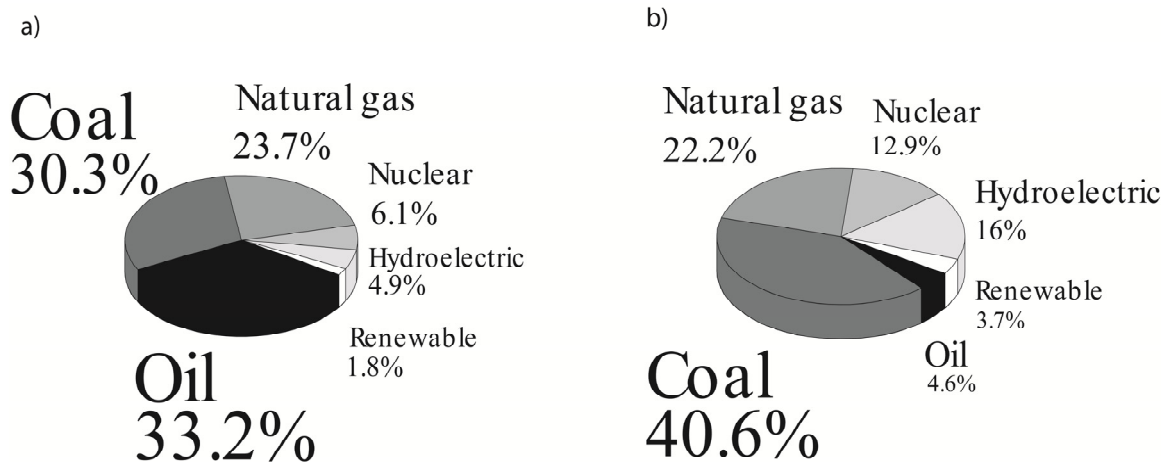


Figure 1.1a) Energy source distribution providing the total world power consumption **b)** Energy source distribution providing the world electrical power consumption

However, two major issues exist regarding the use of fossil fuels as energy source. One issue is that conversion of fossil fuels produces a large amount of greenhouse gases, most importantly carbon dioxide. Whether or not the current global warming is caused by anthropogenic activity alone, a natural effect or a combination of both, it is a fact that CO₂ levels have been fluctuating between constant extremes during several hundred thousands of years before present,^[3, 4] but these extremes have been rising rapidly since the beginning of the industrial age.^[5, 6] Due to the rapid increase of CO₂ concentration, the Kyoto protocol has been developed, which demands lowering of CO₂ emission, and its agreements are based on retaining global warming within a 2 °C rise with respect to the pre-industrial age.^[7]

Another issue is that consumed fossil fuels will not be replenished naturally (to be more precise, this process takes millions of years). The result is a limited amount of recoverable fossil fuels left on Earth. Estimated amounts of recoverable resources are 189 years of oil, 241 years of natural gas and 2780 years of coal.^[2] However, when technical recoverability is taken into account, the estimated times before fossil fuel reserves run out are on average 54-55 years for oil, 64-71 years for natural gas and 112-132 years for coal.^[1, 2] These numbers are optimistically calculated assuming no increase in supply or demand. The final result will be a gap between the total world power production and consumption, which is estimated to be around 14 TW in 2050 and around 33 TW in 2100.^[8]

1.2 Renewable energy sources

To anticipate on both global warming and the upcoming energy shortage, we need to develop new energy technologies based on CO₂-neutral renewable energy sources. Renewable energy is defined as energy derived from a source that constantly replenishes the driving force that is used to generate energy. Thus, candidates for renewable energy sources are nuclear, wind, geothermal, biomass, hydroelectric, tide/ocean and solar energy, each with their advantages and disadvantages. Based on their geographical availability and environmental politics, supplying the world with power will probably be accomplished with a combination of renewable energy sources.

One particularly appealing advantage from solar energy is its enormous energy potential. The Earth receives a stunning 36000 TW on land in the form of sunlight, thereby dwarfing the energy potential of all other renewable energy sources.^[9] It is the only renewable energy source that could supply all the power the world demands, now and in the future. This is the reason why research on solar energy technologies such as solar electric and solar thermal, is so important.

1.3 Economical viability

Besides utilizing a clean and abundant source of energy, a renewable energy technology needs to be cheap. Cost reduction for any kind of new energy technology is important since grid parity, the moment an alternative form of energy reaches the same or lower levelized cost of energy (LCOE, eq. 1) as the source that produces the current grid power, should be achieved before an alternative energy source becomes commercially interesting.

$$LCOE = \frac{\sum_{t=1}^n \frac{I_t + M_t + F_t}{(1+r)^t}}{\sum_{t=1}^n \frac{E_t}{(1+r)^t}} \quad \text{eq. 1}$$

Where t = time (years), I_t = investment expenditures, M_t = operations and maintenance expenditures, F_t = fuel expenditures, E_t = Electricity generation (all in year t), r = discount rate, n = lifetime of a system.

To decrease the LCOE it is preferred to utilize cheap and abundant materials, minimize the amount of material used for fabrication and use a cheap production process while maximizing electricity generation and lifetime. A combination of all these factors is the most beneficial, but as long as the LCOE can be reduced sufficiently, a renewable energy technology has a future as next generation power source. The LCOE of photovoltaics (PV) is at the moment around 2.5 times higher than the LCOE of fossil fuel based electricity,^[10] but technological advances and rising fossil fuels prizes will likely favor this number in the near future.

1.4 The solar spectrum

Earth receives solar emission as a distribution of photons with specific energy, the solar irradiation spectrum. The spectrum that is received at $\sim 48^\circ$ relative to the Earth's normal is standardized as the AM 1.5G solar irradiation spectrum with a total power of 1000 W m^{-2} (Fig. 1.2), which is used to test photovoltaic performance.

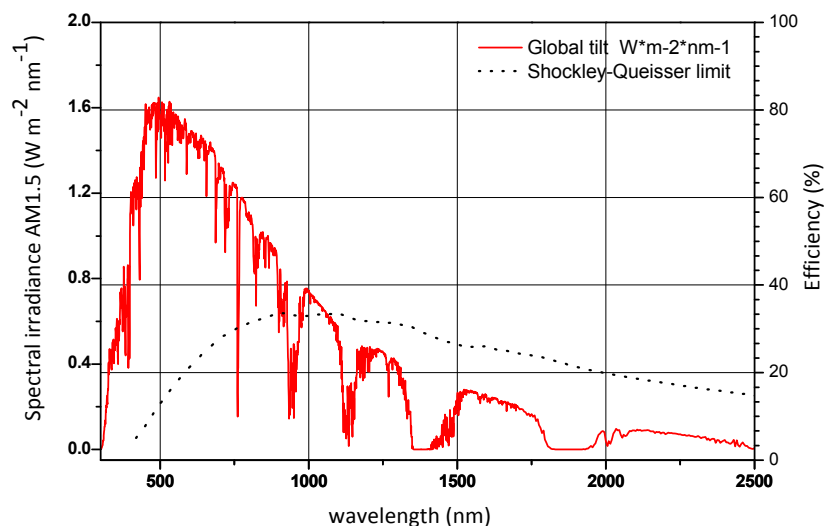


Figure 1.2 Red: Standardized ASTM G-173-07 1.5AM solar irradiation spectrum Black: Shockley-Queisser maximum efficiency limit for a single layer solar cell.

To efficiently utilize solar energy, the semiconductor material in a solar cell needs to be able to absorb a significant portion of the available photons. The property of a material that governs what minimum photon energy can be absorbed is the bandgap (E_g) which needs to be matched by a certain photon energy before absorption occurs. The semiconductor bandgap that potentially offers the highest power output for a single layer solar cell has been described by Shockley-Queisser (Fig. 1.2), and is roughly between 1-1.5 eV or 1250-830 nm.^[11] Preferably, semiconductors combine these optimal bandgaps with broad spectral coverage.

1.5 Silicon solar cells

Nowadays, the most conventional semiconductor for solar cells is crystalline silicon. Silicon has high natural abundance, possesses an optimal bandgap of 1.1 eV and broad spectral coverage from the near IR to the UV-region in the solar spectrum, ideal for the absorption of solar irradiation. Combined with efficient charge generation, silicon based photovoltaics offer high power conversion efficiencies (PCE), 25% on lab scale and 11-16% in commercial arrays,^[12] and lifetimes of about 20 years.

Even though the silicates used for silicon production are abundant and cheap, the requirement of high purity silicon combined with rather thick silicon layers, due to its low optical density, makes silicon-based solar cells relatively expensive. Therefore, new technologies and innovations that reduce material and manufacturing costs need to be investigated. One of these technologies currently under investigation are PVs based on polymer semiconductors.

1.6 Polymer solar cells

Polymers are normally regarded as insulators which are unable to conduct electricity or absorb sunlight. This view changed when conjugated polymers were developed that showed conductivity upon doping. In 1963 McNeill *et al.* reported the first example of doping, rendering a polypyrrole polymer a modest conductivity of 1 S cm^{-1} .^[13] In 1977, work was published by Shirakawa, McDiarmid and Heeger where polyacetylene (PA) (Fig. 1.3a) was doped with iodine, resulting in maximum conductivities of approximately 38 S cm^{-1} .^[14] For their total contribution on the discovery and development of conjugated polymers Shirakawa, McDiarmid and Heeger were awarded the Nobel Prize in 2000.^[15]

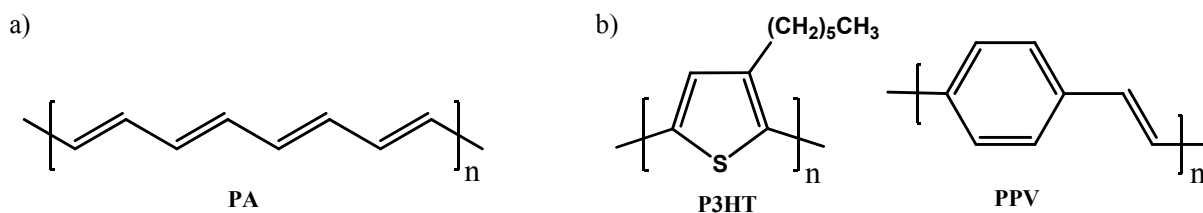


Figure 1.3 a) chemical structure of polyacetylene. Multiple repeating units are drawn for clarity **b)** chemical structures of P3HT and PPV

Their work initiated the intense investigation of conjugated polymers as the semiconductor material in solar cells, light-emitting diodes^[16] and field-effect transistors.^[17] Due to the limited processability, stability and options for chemical modification of PA, the workhorses of the organic electronics community became polymers based on aromatic units; poly(3-hexylthiophene-2,5-diyl) P3HT and poly(phenylene-vinylene) (PPV) derivatives (Fig. 1.3b).

The main advantage of organic photovoltaics (OPV)s is the promise of being solution processed via a cheap and efficient roll-to-roll process, inkjet printing or spray coating.^[18] Additionally, they potentially offer light weight and flexible PV which opens up additional commercial applications. The natural abundance of the main elements needed for production, sulfur, nitrogen, carbon, hydrogen and oxygen is high. Also, organic materials have a high absorption coefficient which reduces the required active layer thickness to ~100-200 nm and therefore the amount of material that is needed for efficient absorption of sunlight. Nowadays, laboratory devices offer the required power conversion efficiencies for commercialization (8-10%)^[19,20]

However, the test areas of these devices are usually on the order of 0.09-1 cm², while efficiencies of OPV in realistically sized photovoltaic cells are much lower, 1-3% PCE for 25-225 cm² area^[21, 22]. Also, thermal, photochemical and long-term stability of OPV's is still inferior compared to PV based on inorganic materials.^[23] Since OPVs require a two-material active layer instead of one (e.g. silicon) to achieve efficient charge generation, it involves a complex interplay of both materials based on their individual properties. This, combined with the physical and opto-electronic properties that are required for efficient solar cells, imposes several design rules on the chemical structure of the polymer. Even the smallest change done on a polymer structure can result in vastly different and often unexpected changes in polymer/device properties. Understanding these structure-property relationships is one important aspect in the research of OPV to ultimately provide a reliable and efficient renewable energy technology.

1.7 Aim of the thesis

The work described in this thesis deals with the design, synthesis and characterization of π -conjugated polymers for solar cells. The focus of this thesis is two-fold; it focuses on both the optimization of several parent structures, mainly by engineering the HOMO, LUMO and bandgap of the polymer materials, but also on establishing structure-property relationships upon alteration of these parent structures.

The synthesis and characterization has been done at Chalmers University of Technology, Göteborg, Sweden, while device characterization has been conducted at IMEC, Belgium. Part of this work was conducted within the EU project ONE-P. This work has been funded by the EU project ONE-P under grant no. 212311 and the Swedish Energy Agency.

Chapter 2

ORGANIC SOLAR CELLS

2.1 Bandgap and excitations

The reason why conjugated polymers are able to absorb sunlight is because of the single-double bond alternation that exists in the backbone. Considering polyacetylene (Fig. 2.1), the backbone consists of tetravalent carbon atoms where three electrons are involved in forming three sp^2 -bonds, two between adjacent carbon atoms and one between the hydrogen.

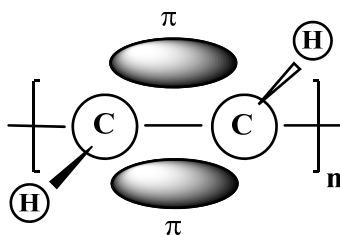


Figure 2.1 schematic representation of the π -conjugated system in polyacetylene

These bonds are located in the centre of the two nuclei and have a σ -bond character. One electron in the p-orbital is left that interacts with another adjacent p-electron from the neighboring carbon atom. This forms the π -bonding or highest occupied molecular orbital (HOMO) and the empty π^* -antibonding or lowest unoccupied molecular orbital (LUMO) (Fig 2.1), that evolve further into a valence (bordered by the HOMO) and conduction (bordered by the LUMO) ‘band’ of closely spaced energy levels in a polymer material. The energy difference between the HOMO and the LUMO is then defined as the bandgap (Fig. 2.2a). Because π -orbitals are located out of plane in the molecule, they are less bound to the carbon nuclei and reduce the photon energy needed for photoexcitation. Upon absorption of a photon with $E_{\text{photon}} \geq E_g$, an electron is photoexcited from the valence to the conduction band creating a bound electron-hole pair, or exciton (Fig. 2.2b), while the σ -bonds maintain the structural integrity of the polymer

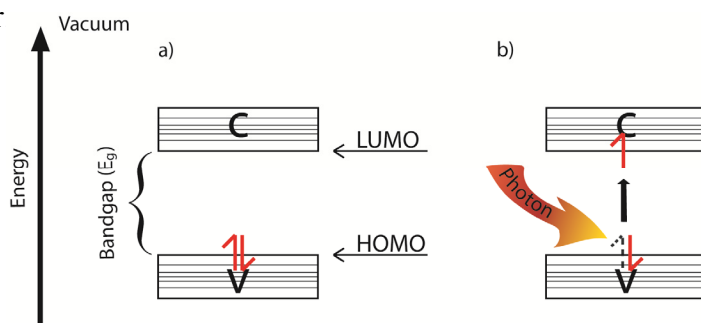


Figure 2.2 **a** Valence (V) and conduction (C) ‘band’, bordered by the HOMO and LUMO respectively and separated by E_g . **b** process of photoexcitation where a photon with $E_{\text{photon}} \geq E_g$ promotes an electron from V to C, creating an exciton.

2.2 Charge generation in organic semiconductors

Charge generation in solar cells occurs in the following simplified way. Upon formation of the exciton it separates into an electron and a hole which are then transported and collected at each of their respective electrodes (Fig 2.3d-1). The difference in work function between the anode and cathode induces an internal electric field that directs the separated charges to each of their respective electrodes.

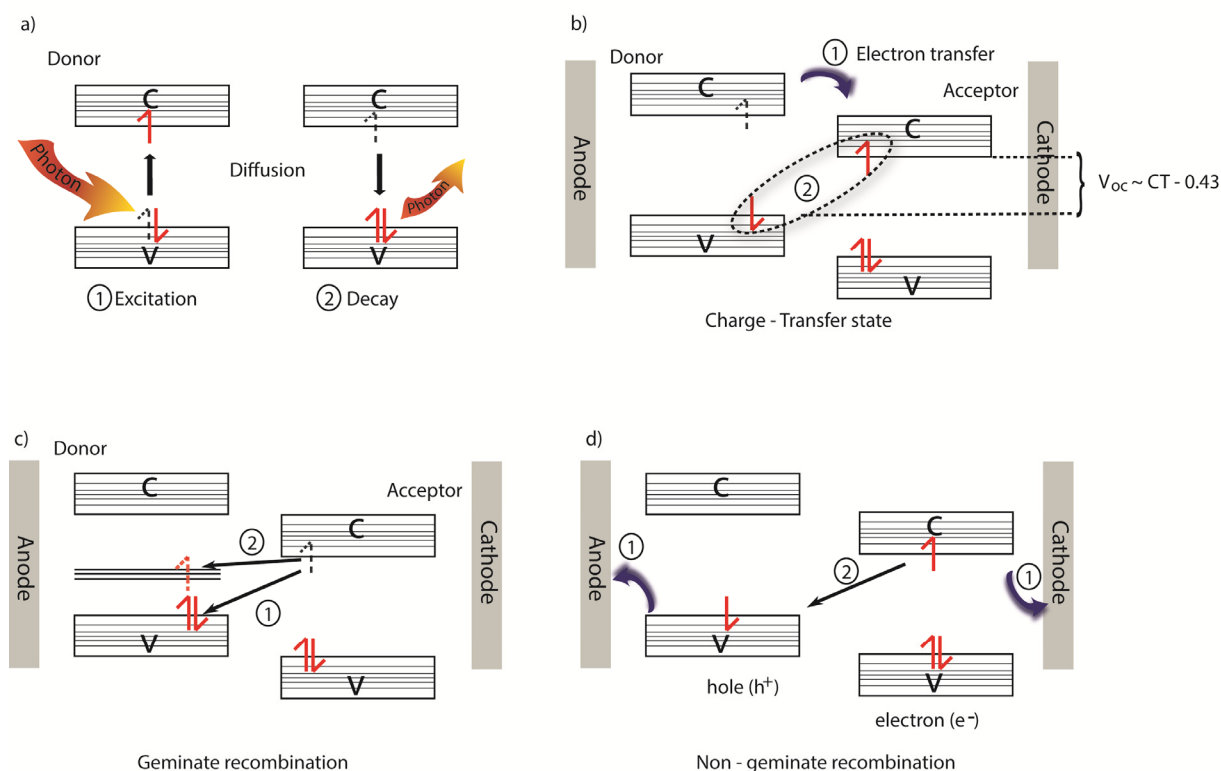


Figure 2.3 Schematic of charge generation in organic solar cells. **a)** Exciton formation(1) and decay(2) **b)** electron transfer from $LUMO_{donor}$ to $LUMO_{acceptor}$ (1) and formation of the CT-state(2), **c)** geminate recombination of the CT-state, either directly to $HOMO_{donor}$ or via the triplet state (2) **d)** generated free charge carriers, either transported and collected at their respective electrodes (1) or recombined non-geminately(2).

Unfortunately, this scenario only applies to inorganic solar cells where the high dielectric constant causes the exciton to be weakly bound, enabling exciton separation into free charges with thermal energy. In organic materials, the dielectric constant is quite low ($\epsilon \sim 3-4$) resulting in a high coulombic attraction between an electron and a hole. Therefore, the exciton remains as this bound electron-hole pair (Fig. 2.3a-1), with an accompanying distortion in the molecular geometry, instead of separating into free charge carriers. This exciton, since it is chargeless, starts to diffuse through the material for approximately 5-15 nm^[24, 25] upon which it radiatively or nonradiatively decays back to a level in the ground state (Fig 2.3a-2). Upon radiative decay, a photon with lower energy is emitted. The energy difference between the

absorbed and emitted photon is the Stokes shift, which is a measure of the energy loss due to molecular vibrations that dissipates as heat.

A solution to enhance exciton separation was put forward by Tang, who combined a phthalocyanine dye as the donor and a perylene tetracarboxylic derivative as the acceptor in a solar cell, offering a PCE of ~1%.^[26] Donor-acceptor induced exciton separation is explained by the relative alignment of the donor and acceptor materials' energy levels, which is shifted more away from vacuum for the latter (higher electron affinity). Upon reaching the donor-acceptor interface the electron in the LUMO of the donor will hop to the LUMO of the acceptor due to the energy difference between the two LUMO's (Fig. 2.3b-1). This process is actually equal but in the opposite direction for holes, as an electron will hop from the HOMO of the donor to the HOMO of the acceptor.

Due to their excellent electron accepting properties, most utilized acceptors nowadays are soluble fullerene derivatives such as [6,6]-phenyl-C₆₁-butyric acid methyl ester (PC₆₁BM) or [6,6]-phenyl C₇₁ butyric acid methyl ester (PC₇₁BM) (Fig 2.4).^[27, 28] Aside from organic small molecules, inorganic materials and polymers have also been employed as acceptors.^[29-32]

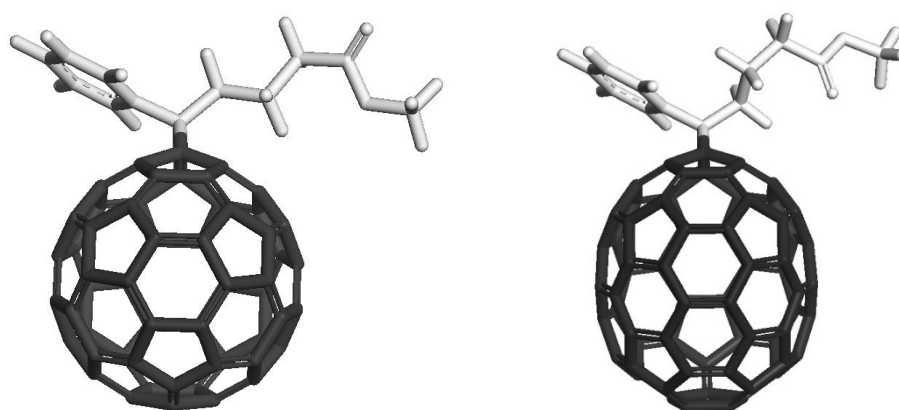


Figure 2.4 chemical structure of [6,6]-phenyl-C₆₁-butyric acid methyl ester (left) and [6,6]-phenyl C₇₁ butyric acid methyl ester (right)

After electron-transfer from the donor to the acceptor occurs, a charge transfer (CT)-state is created (Fig. 2.3b-2) instead of free charge carriers. The CT-state either separates into a free hole and electron that are collected at their respective electrodes, or recombine in a process called geminate recombination, which happens directly (Fig. 2.3c-1) or uses the triplet state as an alternative pathway (Fig. 2.3c-2).^[33-35]

The exact driving force for exciton separation in OPV is still under debate but it was reported that, in general, a larger difference between the respective donor and acceptor

LUMO's resulted in a higher number of charge carriers.^[36, 37] Unfortunately, large LUMO-LUMO differences result in energy loss and limit the performance of organic solar cells. However, exceptions have also been reported where a small LUMO-LUMO difference still resulted in efficient charge generation.^[38, 39] Another property of the CT-state is that its emission energy can be measured, which can be related to V_{oc} generated by an OPV device, $V_{oc} = E_{ct} - \sim 0.43 \text{ eV}$.^[40] The CT-state in turn relates to the $HOMO_{donor} - LUMO_{acceptor}$ difference.^[41]

The generated free charge carriers are then transported via the donor (transporting holes) and acceptor (transporting electrons) phases to their respective electrodes (Fig. 2.3d-1). During charge transport, electrons and holes potentially recombine again in a process called non-geminate recombination (Fig. 2.3d-2).

An issue when using a combination of a donor and an acceptor material is that separated charges are only created at the donor-acceptor interface.^[42] To maximize the donor-acceptor interfacial area, the molecules were combined resulting in an intimately mixed interpenetrating network of a donor and acceptor phase (Fig. 2.5), resulting in improved power conversion efficiency.^[43] This so called bulk heterojunction (BHJ) consisting of a polymer as the main absorber and donor material and PCBM as the acceptor is currently the most utilized active layer in OPV.

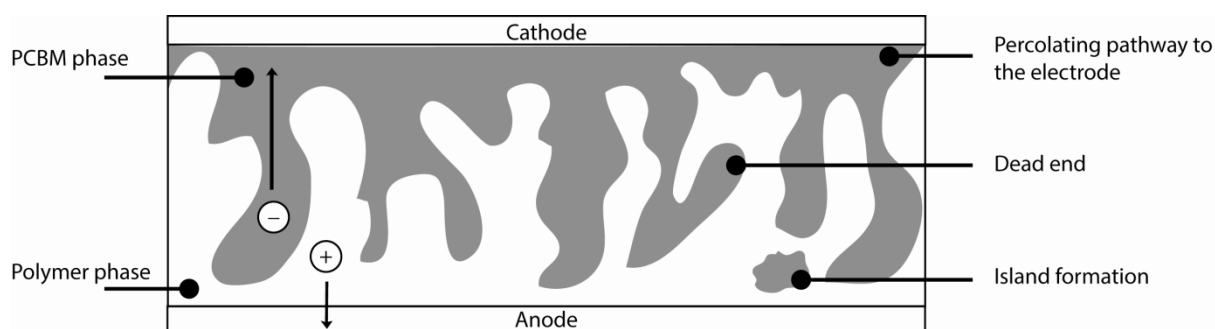


Figure 2.5 Schematic representation of the bulk heterojunction

A donor-acceptor blend imposes rather specific requirements on the domain size and morphology in the blend that, if not met, would amplify loss mechanisms during charge generation and extraction of the generated charge carriers.

If the domain size of these percolating pathways is larger than the exciton lifetime, generated excitons in the donor or acceptor phase will decay before they reach the donor-acceptor interface. Large domains also limit the donor-acceptor interface, reducing the

amount of charge carriers that can be formed while too intimately mixed donor and acceptor phases increase the donor-acceptor interfacial area, that is favored for efficient charge-carrier generation, but also of non-geminate recombination. The relative domain size governs the balance between electron and hole mobility which, if unbalanced, causes a buildup of space charge that increases the probability of non-geminate recombination.

Percolating pathways can, instead of being connected to their respective electrodes, also form so called dead ends or isolated islands (Fig. 2.5), which prevent extraction of the generated charge. Also, fullerene molecules usually exhibit some solubility in the polymer phase, i.e. the fullerene is everywhere.^[44] This can be considered as an extreme case of island formation.

Controlling blend morphology is still a challenge since the active layer is formed via solution processing a mixture of donor and acceptor molecules and introduces parameters that cannot be controlled easily. For instance, solvent, molecular weight, blend ratio of donor and acceptor, solubility, surface energy and processing additives can all influence blend morphology.^[45-51] One possible solution that is explored to control the blend morphology are block copolymers, due to their self-organizing properties.^[52]

2.3 Architecture of organic solar cells and performance parameters

An organic solar cell is generally constructed by stacking different material layers, each with a specific function (Fig. 2.6).

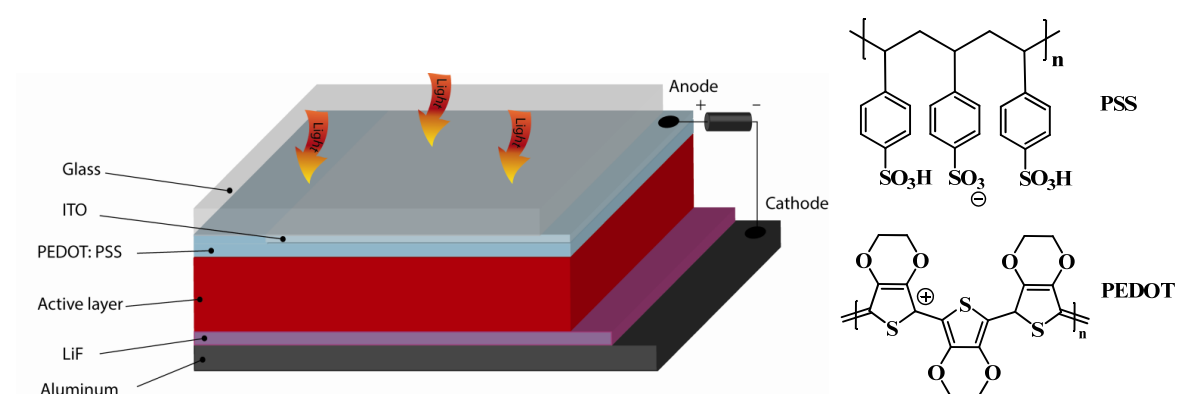
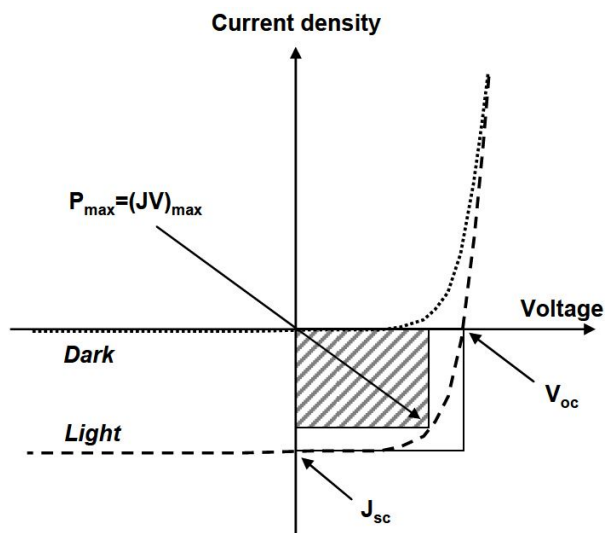


Figure 2.6 Schematic image of the stacked architecture in an organic solar cell

The substrate used for test devices is usually glass, coated with indium-tin oxide (ITO), a transparent anode material with high work function that collects the generated holes. On top of the ITO a water solution of poly(ethylene-dioxythiophene) and poly(styrene-sulphonic

acid) (PEDOT:PSS) is spun, which smoothens the surface of the ITO, facilitates the extraction of holes and decreases the work function of ITO (4.4-4.8 eV) to around 5.0 eV.^[53] The active polymer:fullerene blend layer is deposited on top of these two layers, generally via spin-coating, but blade coating or paint rolling are other options. On top of the active layer is a vacuum-deposited interlayer material, such as lithium fluoride, calcium or ytterbium which is followed by aluminum. These materials form the cathode that collects the generated charge carriers and reflects back the photons not absorbed by the blend.

The power output from solar cells is usually measured under a solar simulator with the standardized AM1.5 solar irradiance spectrum which typically produces $\sim 1000 \text{ W m}^{-2}$. The power conversion efficiency (η), is the percentage power from light irradiation (P_{in}) that is converted into electrical power (P_{max}). P_{max} is built up out of three parameters, the short-circuit current density (J_{sc}), the open-circuit voltage (V_{oc}) and the fill factor (FF) (eq. 2) and generally depicted in the form of an IV-curve (fig 2.7).



$$\eta = \frac{P_{max}}{P_{in}} = \frac{FF * J_{sc} * V_{oc}}{P_{in}} \quad \text{eq. 2}$$

$$\text{Where } FF = \frac{P_{max}}{J_{sc} * V_{oc}}$$

Figure 2.7 Current density-voltage curve for a photovoltaic cell under illumination (dashed line) and in the dark (dotted line). The ratio between the filled and blank square gives the fill factor of the solar cell.

The J_{sc} is the maximum amount of electrons that a device is able to generate at zero bias. Generally, the bandgap, spectral coverage and absorption coefficient of a material determines how many photons from the solar spectrum are absorbed. Aside from the loss mechanisms due to utilization of the active donor-acceptor blend, there are additional loss mechanisms that can limit the J_{sc} such as incomplete absorption of sunlight due to scattering at the interface or too thin active layer thickness that limits the amount of light that can be absorbed.

The maximum V_{oc} of a photovoltaic device is generally determined by the difference in the electrodes' workfunctions. However, if the energy levels of the active blend material are located within these workfunctions, the maximum V_{oc} is determined by the energy difference between the LUMO of the acceptor and the HOMO of the donor. Reduction of V_{oc} can occur due to poor contact between the electrode and active layer, interactions between the active layer and the electrode, or via severe recombination.

The fill factor is a parameter calculated by the ratio between the maximum possible power $J_{sc} \times V_{oc}$ and P_{max} . The closer FF is to unity the more a solar cell acts as an ideal electrical component.

2.4 Designing materials for organic solar cells

From the previous section a couple of important properties for conjugated polymers can be identified that determine the efficiency of the final bulk heterojunction solar cell.

Polymers require solubility in the commonly used processing solvents such as chloroform, chlorobenzene and dichlorobenzene, generally achieved by attaching flexible alkyl side chains to the rigid backbone. Also, although difficult to predict and therefore manipulate, interactions between polymer, fullerene and solvent determine the blend morphology to some extent, which concomitantly determines charge generation and extraction.

However, for this work the most important parameter is the energy level alignment of the polymer. The position of the polymers' energy levels determines the maximum achievable PCE via the bandgap, whereas the relative alignment of the polymer donor and acceptor energy levels determines charge generation efficiency and maximum V_{oc} . The acceptor in most cases is a PCBM derivative, so polymer bandgap and energy levels are commonly varied with the energy levels of the fullerenes as reference.

As already mentioned, polyacetylene has poor processability and limited options for chemical modifications. Therefore polymers based on aromatic rings have been developed which enables numerous chemical modifications. The energy levels of these aromatic polymers can be manipulated by a number of design strategies, which are summarized in Figure 2.8.

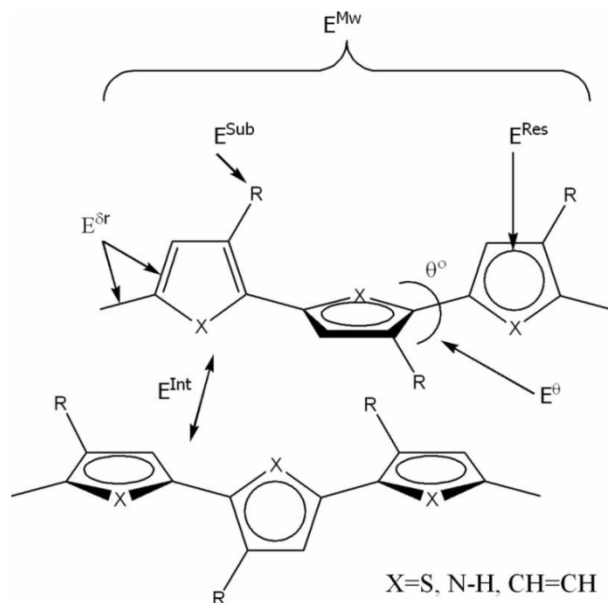


Figure 2.8 Parameters influencing the band gap (E_g): molecular weight (M_w), bond length difference (δ_r), resonance energy (Res), substituents (Sub), dihedral angle (θ), and interchain effects (Int).

Increasing conjugation length (**Mw**) is a relative straightforward way of manipulating the bandgap in a conjugated polymer. An example is given in Figure 2.9, where the energy levels of an ethylene molecule are displayed as function of the amount of repeating units.

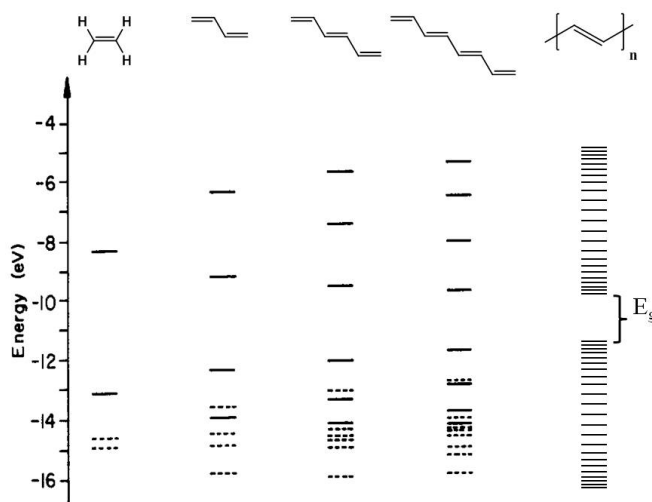


Figure 2.9 Evolution of the bandgap in polyacetylene as function of the amount of repeating units. Picture adopted from ref^[54]

Combining two or more of these ethylene molecules results in orbital overlap of their bonding and antibonding orbitals, which creates new molecular energy levels. Their position relative to vacuum is determined by the amount of orbital overlap. Upon adding more units, the effect of each added unit on the bandgap saturates. Obtaining appropriate molecular weight requires

high monomer purity and polymer solubility, which is generally achieved by adding more or longer alkyl side chains, but can also be done by reducing backbone stiffness.

The parameter δ_r corresponds to the difference in length between the single and double bonds in a conjugated polymer. It can be rationalized by considering polyacetylene as a polyradical ($-C^*-$) with equal bond lengths between each repeating unit, which would make it a conductor (zero bandgap). Due to the interaction of two adjacent π -orbitals, bond length alternation or Peierls distortion is induced, which results in longer (single) or shorter (double) bonds and makes polyacetylene a semiconductor. Therefore, if the difference in single and double bonds is reduced the bandgap becomes smaller i.e. the more delocalized the electrons are, the smaller the bandgap will be. When considering for instance a polyaromatic like poly-paraphenylene (PPP) (Fig 2.10a), two resonance forms can be drawn; the aromatic form which is lower in energy and the quinoid form, which is higher in energy with a smaller δ_r . Therefore, if the quinoidal form can be stabilized by reducing δ_r the bandgap becomes smaller.

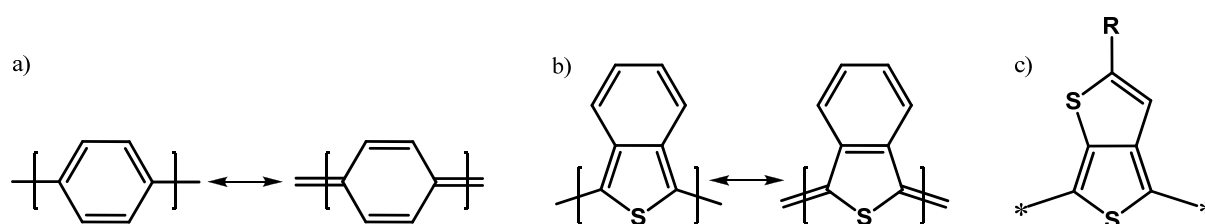


Figure 2.10 a) equilibrium between aromatic and quinoidal form in PPP b) equilibrium between aromatic and quinoidal form in PITN, c) chemical structure of the thieno[3,4-*b*]thiophene moiety

Generally, two strategies are employed to stabilize the quinoidal form. The first can be described as the approach used in polyisothianaphthalene (PITN, Fig 2.10b). In PITN the quinoidal form is more stable than the aromatic form due to the higher aromaticity of benzene, which by adopting its aromatic form automatically induces more double bond character in the bonds between the monomers, resulting in a small bandgap of ~ 1 eV.^[55] More recently, a series of polymers utilized this effect by incorporating thieno[3,4-*b*]thiophene monomers which offered $\sim 7\%$ PCE when employed in BHJ solar cell (Fig. 2.10c).^[56]

A different theory that was suggested to stabilize the quinoid form uses the so-called donor-acceptor (D-A) approach in the polymer backbone.^[57] The principle is based on combining an electron-rich monomer (donor) with an electron-poor monomer (acceptor). The donor-acceptor combination induces an intramolecular charge transfer resulting in more double bond character between the monomers, stabilizing the quinoidal form and therefore results in a smaller bandgap (Fig. 2.11a).

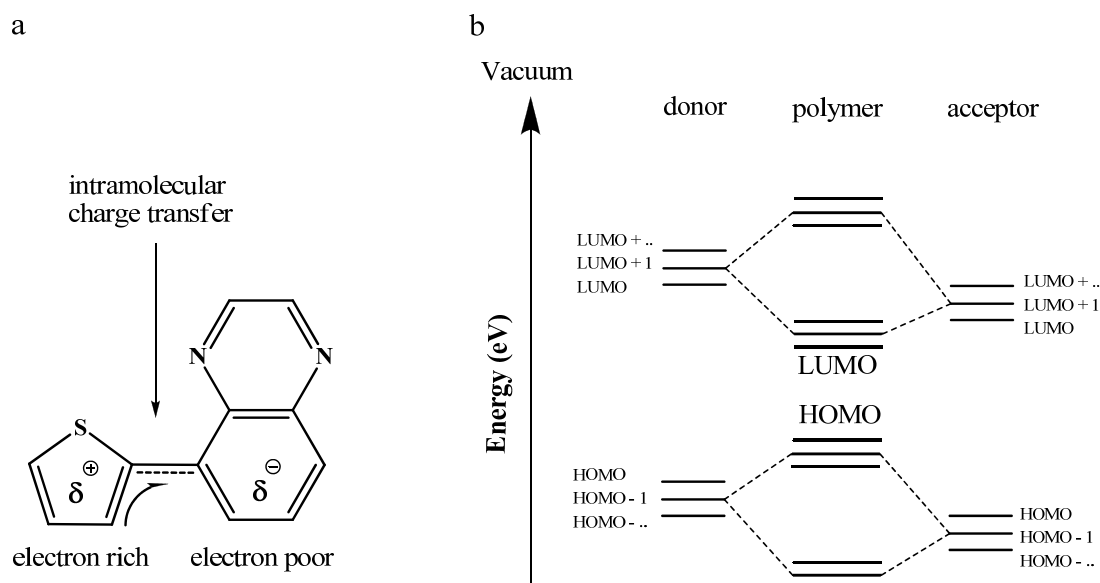


Figure 2.11 a) interaction of an electron-rich unit with an electron-poor unit resulting in partial charge transfer
b) Simplified orbital representation of the donor-acceptor principle.

The D-A approach can also be explained by means of an orbital diagram (Fig. 2.11b). An acceptor unit has its HOMO and LUMO energy levels shifted away from vacuum, relative to the energy levels of the donor unit. In an oversimplified picture, the energy levels of the polymer will resemble the HOMO closest to vacuum (usually from the donor) and the LUMO most shifted away from vacuum (usually from the acceptor). This also means that with some combinations of donors and acceptors, an aromatic monomer merely acts as a π -conjugated spacer. By selecting different combinations of donors and acceptors the bandgap and position of energy levels in a polymer can be varied indefinitely.

However, the energy difference between corresponding donor and acceptor energy levels determines the amount of overlap. For instance, when HOMO's of donor and acceptor overlap well it will shift the polymer HOMO towards vacuum. Conversely, a large difference between the LUMO of the donor and the LUMO of the acceptor results in the LUMO of the polymer being mostly governed by the acceptor.

Another factor governing conjugation length is the dihedral angle (θ) between adjacent monomers, or coplanarity. Coplanarity between adjacent monomers increases conjugation length and delocalization of electrons along the backbone, hence resulting in a smaller bandgap. This effect can be seen in the UV-Vis absorption of dilute polymer solutions as function of solvent quality or temperature, which results in more disordered chain conformations and therefore a blueshifted UV-vis absorption.^[58, 59] To reduce the dihedral angle, various fused units with an increasing number of rings and thiophene terminals have

been incorporated in photovoltaic polymers to improve the conjugation length while reducing the dihedral angle.^[56, 60-63] Aside from reducing dihedral angle and bandgap, incorporating fused units could potentially improve charge generation by extension of the exciton and reducing its binding energy.^[64]

Competition exists between confinement of π -electrons in the aromatic unit or along the backbone of the polymer, expressed as resonance energy (**Res**), which influences the bandgap. For instance, the aromaticity was calculated showing pyrrole>thiophene>furan^[65] However, the corresponding polymer series shows decreasing bandgaps going from polypyrrole>polyfuran>polythiophene.^[66] The influence of the heteroatom and the stability of the system on the bandgap also have to be taken into account.

Any substitution (**Sub**) done on the polymer backbone has an electron-donating or withdrawing effect and can be employed to fine-tune the position of the energy levels. Alkyl or alkoxy side chains, which are often used to improve solubility, have an electron donating effect while fluorine, carbonyl or cyano groups act as electron withdrawing groups.^[67] Depending on the nature of the substitution or the substitution site (donor or acceptor), either the HOMO or LUMO of the polymer is shifted more towards or away from vacuum.

Substitutions done in the form of alkyl chains are usually done to alter the solubility or solid state aggregation of the polymer. By using more or longer alkyl chains the solubility of a polymer can be improved, which would result in a higher molecular weight. Also, the use of branched side chains can alter the packing of polymer chains and thereby influence the bandgap. Aside from affecting the bandgap, alkyl side chains can be used to alter miscibility and phase behavior of the polymer-fullerene blend, intercalation or polymer backbone orientation.^[68, 69]

As the delocalization of electrons will lower the bandgap, extending delocalization over more than one polymer chain (**Int**) either via solid state aggregation or crystallization also results in a smaller bandgap. An example can be found in poly-(3-hexylthiophene) (P3HT). In solution it exhibits an absorption onset of ~560 nm but in solid state a redshift to 650 nm is observed.^[70] The extent to which P3HT aggregates/crystallizes is enhanced by the regioregularity of the repeating 3-hexylthiophene monomers (dihedral angle) and the molecular weight.^[71-73] Annealing also has a profound effect on the performance of P3HT:PCBM BHJ solar cells, leading to a dramatic improvement in PCE.^[74]

Even though various chemical modifications can be done on a polymer structure, it is well established that structure-property relationships are highly entangled. One structural

modification can affect numerous material properties, thus making such relationships hard to define.

2.5 Outline

Chapter 3 will describe the synthesis and properties of several silafluorene-based copolymers. A comparison has been made between fluorene and silafluorene based copolymers, which show very similar optical and redox properties and photovoltaic performance in polymer: PC₆₁BM/PC₇₁BM BHJ solar cells while the thermal behavior of the polymers changed significantly.

In Chapter 4 several structural modifications on TQ1 are presented, a parent polymer that offers high PCE in BHJ solar cells. The aim of this study was to investigate synthetic modifications that ultimately lead to higher PCE than TQ1. In section 4.2 some modifications on the acceptor are described which retain the backbone structure and phenyl side groups, with the goal of obtaining an absorption redshift while retaining a high V_{oc} .

Even though the stronger acceptors studied here offer higher V_{oc} , J_{sc} is supposedly limited by the smaller $LUMO_{polymer}-LUMO_{PCBM}$ difference, morphological effects cannot be ruled out.

In Section 4.3 the alkoxyphenyl side group in the TQ1 structure is substituted for alkylthiophene. Aside from an absorption redshift the HOMO is shifted towards vacuum, which potentially limits V_{oc} . It is shown that the electron-donating effect of the thiophene on the HOMO of the polymer can be mitigated by the introduction of electron-withdrawing groups, which lead to an additional absorption redshift combined with a deep HOMO level. Additionally, some unexpected structure-property relationships are found in the work described in section 4.2 and 4.3

Section 4.4 describes the synthesis, properties and photovoltaic performance of a range of polymer structures based on the quinoxaline acceptor in TQ1.

In section 4.5 the performance of TQ1 and one of its derivatives in electrochromics is reported. Optical contrast is still the highest for TQ1, while the TQ1 derivative shows an improved contrast retention at faster switching times, possibly due to a more open polymer morphology.

Chapter 5 describes the effect of alkoxy substitutions on various properties of the previously reported PDPPTPT polymer. It was found that alkoxy substitutions offer increased flexibility in the polymer which improves solubility and reduces T_m , while solid state order was decreased. However, methoxy substituted oligomers actually show higher T_m/T_c than

oligomers based on the parent structure. Arguably, this effect is counteracted due to the larger conformational distribution in the alkoxy polymers. BHJ solar cells based on the alkoxy substituted polymers blended with PC₇₁BM show lower PCE than PDPPTPT based solar cells, a result of reduced V_{oc} and different blend morphology. PDPPTPT was also used as donor material in polymer:PbS hybrid solar cells to clarify charge separation dynamics. In this study, hybrid solar cells based on PDPPTPT and PbS active layers offered good performance of 2.9%.

Chapter 6 concludes the results described in this thesis and puts them in a somewhat broader perspective.

Chapter 3

SILAFLUORENE-BASED COPOLYMERS

3.1 Introduction

In 2008 a silafluorene analogue of APFO-3 was reported (Fig. 3.1a). A copolymer based on 5,5-dioctyl-5H-dibenzo[b,d]silole and the D-A-D structure 4,7-di(thiophen-2-yl)benzo[c][1,2,5]thiadiazole (Fig. 3.1a) displayed a high power conversion efficiency in BHJ solar cells.^[61, 75]

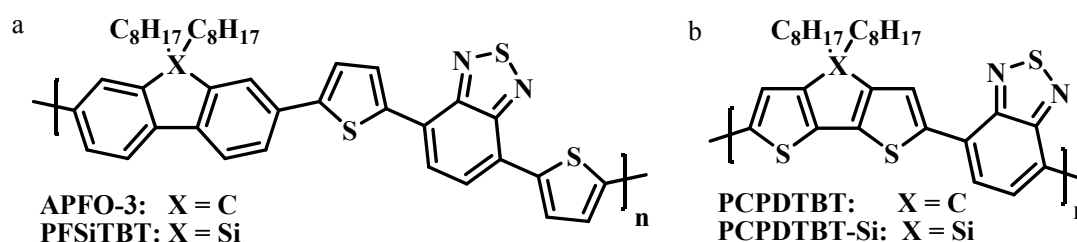


Figure 3.1 chemical structures of a) APFO-3 and PFSiTBT, b) PCPDTBT and PCPDTBT-Si

The interaction of the Si σ^* -orbital with the π^* -orbital of a diene was suggested to increase conjugation along the polymer backbone which would improve charge carrier mobility.^[76, 77] Additionally, the carbon-silicon exchange improves oxidative stability.^[78, 79] Later on, various groups compared the effect of carbon-silicon substitution on the solid state ordering of PCPDTBT (Fig 3.1b), which seems to be influenced significantly by the longer Si-C bond length. As a result, it was found that when the carbon bridging atom in the cyclopentadithiophene moiety was substituted for silicon, solid state interaction improved which manifested itself in additional vibronic features in UV-Vis absorption and X-ray diffraction patterns, indicating π - π stacking which was absent in PCPDTBT^[80, 81]. However, when the 2-ethylhexyl side chains in PCPDTBT were replaced with linear dodecyl side chains, both polymers showed increased order but in this case, the UV-Vis absorption of the polymer incorporating the carbon bridge was redshifted.^[82]

The interesting properties that arise from the carbon-silicon exchange initiated the research on a series of materials in our group, mainly based on the polymers APFO-18 and the narrow bandgap APFO-green9 (Fig 3.2), which at that time showed promising photovoltaic performance.^[83, 84] Aside from the synthesis and properties of these materials a comparison was made between the properties of fluorene and silafluorene-based polymers.

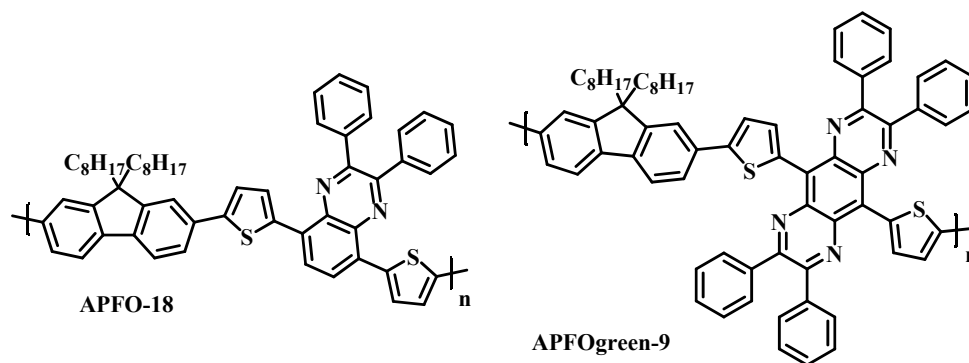
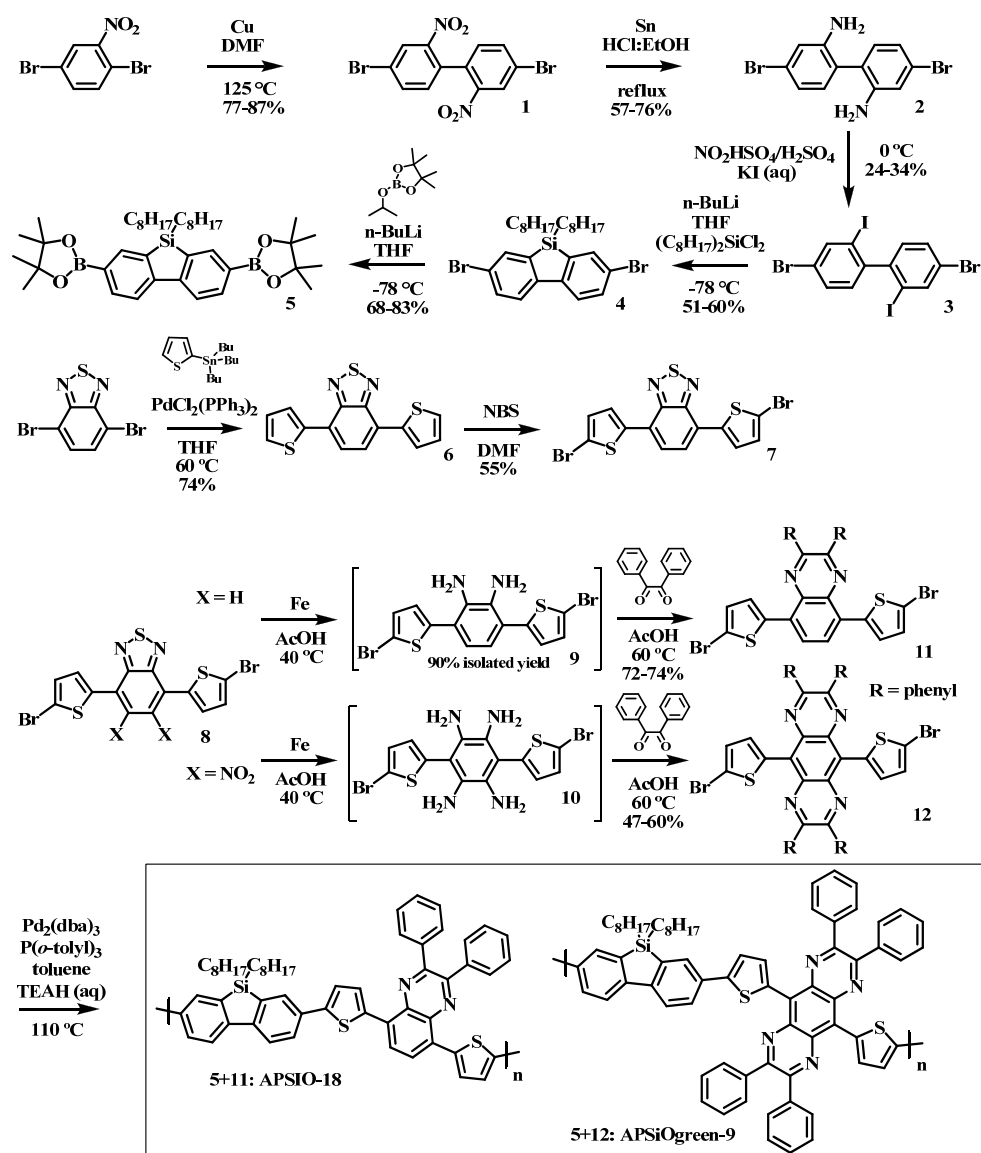


Figure 3.2 chemical structures of APFO-18 and APFO-green9

3.2 Synthesis

The synthesis route towards the polymers (Scheme 3.1) starts with the silafluorene diboronic ester synthesis, where an Ullman coupling of 1,4-dibromo-2-nitrobenzene forms compound **1**, which is then subjected to reduction to form **2**. The amino groups from compound **2** are then transformed via a Sandmeyer reaction to 4,4'-dibromo-2,2'-diiodobiphenyl (**3**). Reaction with *n*-butyllithium selectively lithiates on the 2,2'-iodo position and subsequent reaction with dichlorodioctylsilane results in the silole compound **4**. After lithiation and reaction with 2-isopropoxy-4,4,5,5-tetramethyl-1,3,2-dioxaborolane monomer **5** is obtained. The D-A-D segments are synthesized starting from 4,7-dibromobenzo[*c*][1,2,5]thiadiazole, which is reacted with tributyl(thiophen-2-yl)stannane via Stille coupling to afford compound **6**. Compound **6** is also used as the intermediate for the dinitro derivative which are both brominated with NBS, resulting in compounds **7** and **8**. Reduction of these compounds gives the diamine or tetraamine intermediates **9** and **10**, which are condensed with benzyl to offer the D-A-D segments **11** and **12**. Suzuki polymerization of **5** and either **11** or **12** offers APSiO-18 and APSiO-green9.

Various batches of APSiO-18 and APSiO-green9 have been synthesized in order to obtain reasonable to high molecular weights. As a side note, several attempts were made to synthesize a polymer based on APSiO-18 where the phenyl side groups are substituted with thiophene, to improve solid state interaction. In all cases either low molecular weight or insoluble polymers were obtained, likely resulting from increased intermolecular interactions due to reduced steric hindrance induced by the thiophene side group.



Scheme 3.1 Synthetic scheme leading to APSiO-18 and APSiOgreen-9

3.3 Physical and opto-electronic properties

For most polymers, thermal transitions were observed except for APSiO-green9 who's thermal stability limits the differential scanning calorimetry (DSC) temperature range (Table 3.1). Considering the glass transition temperature (T_g) of the APFO polymers, for APFO-3 with similar molecular weight a value of ~ 100 °C was determined.^[48] When considering a series of APFO-3, APFO-18 and APFO-green9, the T_g of the polymers seems to increase with the amount of bulky phenyl side groups attached to the backbone. Even though a T_g could not be recognized for the APSiO polymers, APSiO-18 does however show several high-temperature transitions, two endotherms on heating and one exotherm on cooling.

Table 3.1: Physical, optical and redox properties of TQ derivatives

Polymer	M_n^a (kg mol^{-1})	PDI	TGA ^b (°C)	T_g^c (°C)	T_{endo} (°C)	T_{exo} (°C)	$E_{g,\text{opt}}^d$ (eV)	E_{HOMO}^e (eV)	E_{LUMO}^e (eV)
APSiO-18 (LMW)	15	3.3	398		272 (1) 333 (2)	265	1.95	-5.52	-3.46
APSiO-18 (HMW)	27	4.7	420				1.94	-5.50	-3.45
APFO-18	8	2.2	310	142			1.96	-5.55	-3.44
APSiO-green9	8	2.2	340				1.42	-5.47	-4.04
APFO-green9	11	2.3	404	192			1.43	-5.53	-4.17

^a Measured against polystyrene standards in trichlorobenzene at 135 °C, ^b 1% weight loss under N_2 , ^c T_g determined from the 2nd heating scan, ^d from peak onset, ^e calculated via peak onset, $-(E_{\text{red/ox}} + 5.13)$

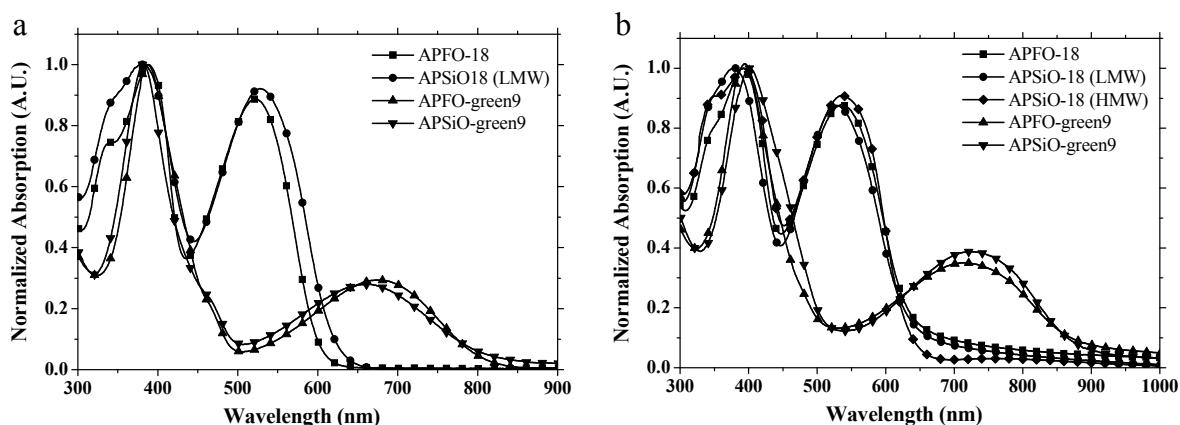


Figure 3.3 a) CHCl_3 solution UV-Vis absorption spectra of APFO and APSiO –polymers and b) solid state UV-Vis absorption spectra, spincoated from CHCl_3 :APFO/APSiO solutions.

All polymers show similar solid state/solution UV-Vis absorption and absorption redshifts when going from solution to solid state (Fig 3.3a and b) and similar oxidation/reduction potentials (Table 3.1). Interestingly, even though the molecular weight of APFO-18 is lower than the low molecular weight APSiO-18 it shows a larger redshift when going to solid state. When taking the molecular weight differences into account, it seems that the effect of carbon-silafluorene substitution on the energy levels and absorption is minimal. To investigate if any additional solid state order could be induced which could explain the difference in thermal behavior, polymer films were made from APFO-18 and APSiO-18 via dropcasting with a slow evaporating solvent, o-DCB. No change in solid state absorption of APFO-18 and APSiO-18 was observed when comparing UV-Vis absorptions from fast drying spincoated CHCl_3 films and slow evaporating dropcasted o-DCB films (not shown). The absence of any change in the UV-Vis absorption spectrum, where additional order would manifest itself as a change in the absorption, suggests no additional order can be induced in either of the polymers.

It was reported that for PCPDTBT and Si-PCPDTBT, the varying C-C and C-Si bond length was found to influence backbone curvature. If the normal is drawn for both the CPDT or Si-CPDT and the adjacent BT acceptor, the angle formed by CPDT and BT is 10° while the angle for Si-CPDT and BT is 24°. [85] The effect of backbone curvature was also investigated for a number of polymers, which show improved solubility but decreased solid state order with increasing backbone curvature. [86] Therefore an explanation for the difference in thermal behavior between the APFO and APSiO polymers could perhaps be found investigating this parameter.

3.4 Photovoltaic performance

Each polymer has been tested in combination with fullerene derivatives in BHJ solar cells. The results are summarized in Table 3.2.

Table 3.2 Photovoltaic data of optimized devices based on polymer: PC_[x]BM blends

Material	Polymer: PC _[x] BM (w:w)	PC _[x] BM	Thickness (nm)	J _{SC} (mA cm ⁻²)	V _{OC} (V)	FF	η (%)
APSiO-18 (LMW)	1:2	60	80	4.5	4.89	0.43	1.7
	1:2	70	80	5.8	0.89	0.45	2.3
APSiO-18(HMW)	1:1	60	60	5.8	0.92	0.48	2.5
	1:1	70	56	8.2	0.89	0.42	3.1
APFO-18	1:4	60	60	4.3	0.94	0.51	2.1
	1:4	70	60	5.3	0.97	0.57	2.9
APSiOgreen-9	1:4	60	70	3.0	0.85	0.34	0.9
	1:4	70	70	5.4	0.85	0.34	1.5
APFOgreen-9	1:4	60	80	4.8	0.82	0.44	1.6
	1:3	70	70	6.5	0.81	0.44	2.3

APSiO-based device architecture ITO/PEDOT:PSS/active layer/Yb/Al, APFO-based device architecture ITO/PEDOT:PSS/active layer/LiF/Al, from o-DCB, from CHCl₃, photovoltaic data for APFO-based devices from ref [83, 84]

Significant effort was put in optimizing APSiO-18 on molecular weight (low/high), solvent (CHCl₃, CB, o-DCB), (blend ratio (1:1 to 1:4 polymer: PC_[x]BM) , processing agent (w or w/o 1,8-octanedithiol), layer thickness (56-145 nm), thermal annealing (w or w/o 10 min annealing at 130 °C) and fullerene derivative (PC_[61]BM, PC_[71]BM or bis-PC_[62]BM). A combination of thin blend layers consisting of the higher molecular weight APSiO-18 in a 1:1 weight ratio with PC₇₁BM spun from o-DCB gave the best photovoltaic performance.

Thermal annealing had no significant effect on the performance while the addition of 1,8-octanedithiol improves V_{oc} and FF slightly, but lowered J_{sc} . Devices based on APSiO-18 are characterized by high V_{oc} , reasonable J_{sc} but unfortunately low FF which ultimately resulted in an efficiency of 3.1%.

APSiOgreen-9 based devices are again characterized by high V_{oc} but moderate J_{sc} and FF. The J_{sc} is likely caused by the small $LUMO_{polymer}-LUMO_{PCBM}$ offset although morphological issues cannot be ruled out. Devices show improvement in PCE when using PC₇₁BM as the acceptor and 1,8-octanedithiol as the processing agent which improves J_{sc} but, compared to devices fabricated without 1,8-octanedithiol, lowers the FF.

Comparing the photovoltaic performance of the fluorene and silafluorene copolymers it seems that the silafluorene based copolymers exhibit similar PCE. The FF seems to be a bit higher for fluorene-based copolymers but these variations could also be caused by different device geometries or fabrication (o-DCB for silafluorene-based polymer devices, CHCl₃ for fluorene-based polymer devices). The results show that, upon exchanging the bridging carbon atom in the fluorene with a silicon atom, optical, redox and photovoltaic properties are similar while the thermal properties are markedly different.

Chapter 4

TQ1 DERIVATIVES

4.1 Introduction

Over the past few decades there has been significant synthetic research on conjugated polymers in order to improve the efficiency of organic solar cells. A common method to achieve improvement in photovoltaic efficiency is through energy level engineering of a (usually well performing) parent structure thereby optimizing the bandgap and energy level alignment of the polymer donor and fullerene acceptor. As already mentioned, structure-property relationships are highly entangled so it is often favorable to employ small structural alterations, ensuring that properties of the resulting materials do not largely differ from the properties of the parent structure. This potentially facilitates explaining various differences in properties between different materials.

An example of such a well performing parent structure is the conjugated polymer poly[2,3-bis(3-(octyloxy)phenyl)quinoxaline-alt-thiophene] (**TQ1**) (scheme 1). TQ1 is an alternating copolymer based on an alkylated quinoxaline acceptor and a thiophene donor, resulting in an optical bandgap of 1.7 eV which is combined with a deep HOMO level. Photovoltaic cells incorporating an active blend layer consisting of TQ1 and PC₇₁BM exhibit rather good PCE, where here cells achieve efficiencies of around 6%, with $V_{oc} = 0.9$ V, $J_{sc} = 10.5$ mA cm⁻² and $FF = 0.64$.^[87, 88] The success of this rather simple polymer structure inspired us to perform small structural alterations on the acceptor structure in order to achieve a more optimal bandgap (1.1-1.5 eV) while retaining a deep HOMO to potentially improve the PV performance. This chapter deals with the structural alterations done on the parent TQ1 polymer and how the structure-property relationships of the resulting polymers evolve.

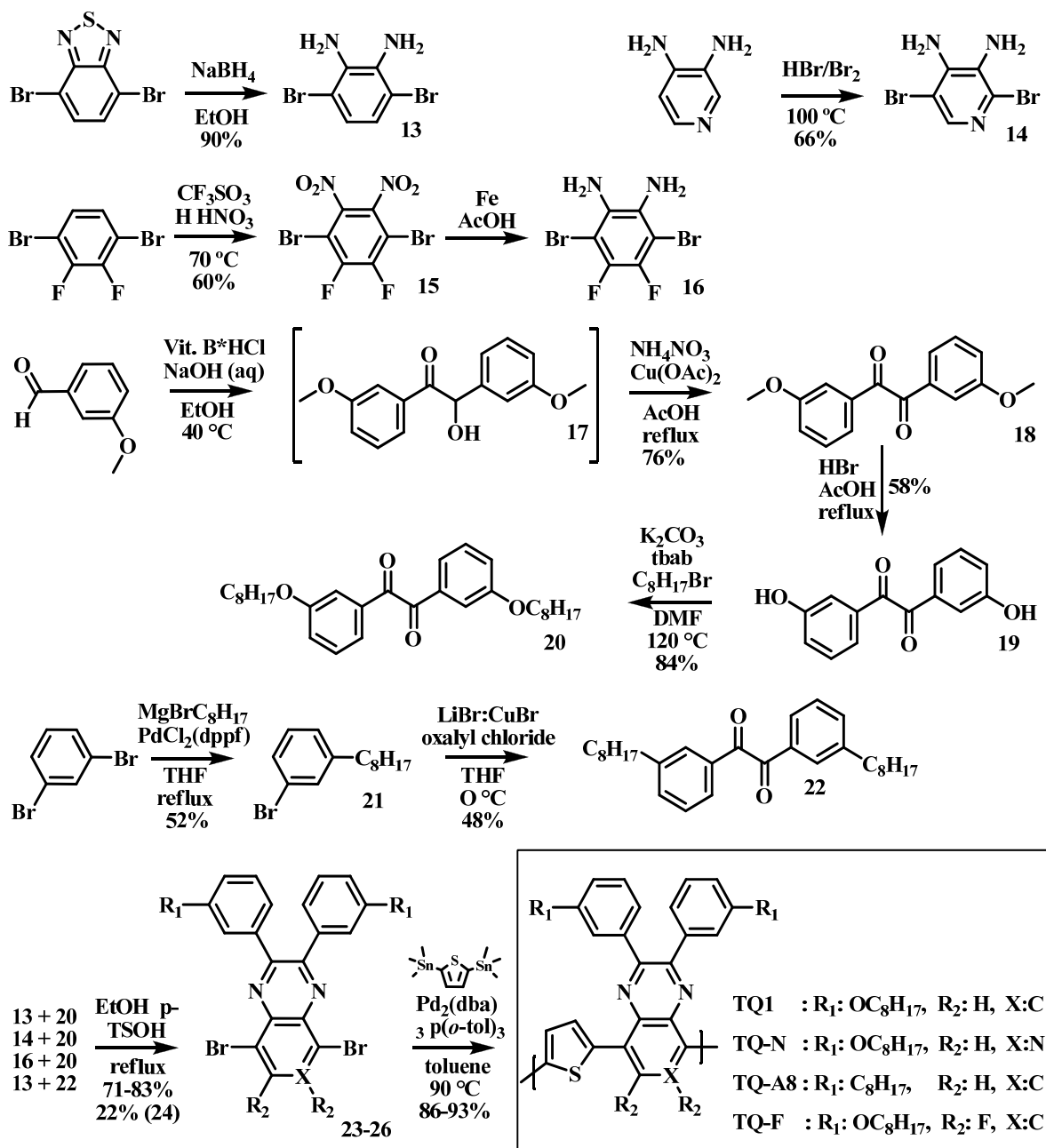
4.2 Acceptor modifications on TQ1

The initial research focuses on modifying (**paper I**) the backbone structure of TQ1 by varying the acceptor strength of the quinoxaline acceptor, mainly with the aim to improve both V_{oc} and J_{sc} . By using a stronger acceptor the bandgap of the polymer will be reduced, thus enabling the harvesting of more photons by the polymer:fullerene blend. Also, V_{oc} could be improved due to the increase in $LUMO_{PCBM} - HOMO_{polymer}$. Enhancement of the acceptor

strength was performed by introducing an additional electron withdrawing imine nitrogen in the acceptor, yielding poly[2,3-bis(3-(octyloxy)phenyl)pyrido[3,4-b]pyrazine-alt-thiophene] (**TQ-N**). A different way of enhancing acceptor strength was done by substituting the two acceptor protons in the backbone with electron withdrawing fluorine atoms, yielding poly[6,7-difluoro-2,3-bis(3-(octyloxy)phenyl)quinoxaline-alt-thiophene] (**TQ-F**). To investigate to what extent the oxygen influences the properties of TQ1, the alkoxy sidechain was replaced with an octyl sidechain, resulting in poly[2,3-bis(3-(octyl)phenyl)quinoxaline-alt-thiophene] (**TQ-8A**).

4.2.1 Synthesis

The synthetic route towards the polymers is depicted in scheme 4.2. The final synthetic step to create the quinoxaline monomers involves condensation of various diamine and α -diketones. Reduction of 4,7-dibromobenzo[c][1,2,5]thiadiazole with NaBH₄ offers diamine **13** which is used for the TQ1 and TQ-8A monomers, while bromination of 3,4-diaminopyridine offers compound **14**. We found that nitration (**15**) and subsequent reduction of 1,4-dibromo-2,3-difluorobenzene to compound **16** is more convenient than the previously reported synthetic route, which involves reduction of 4,5-difluoro-2-nitroaniline and subsequent bromination via activation of the 3- and 6- position with a trimethylsilyl group. One of the problems in the synthesis of diketone **20** is the benzoin condensation used to form the α -hydroxyketone **17**. The reaction is usually performed utilizing the toxic sodium cyanide as catalyst, but has now been replaced with vitamin B1, to offer the same α -hydroxyketone **17** in satisfactory yields (assumed from the yield of compound **18**) without the toxicity of NaCN. After oxidation of α -hydroxyketone **17**, α -diketone **18** was obtained which was subjected to a deprotection to compound **19** that was alkylated through Williamson etherification to offer diketone **20**. Synthesis of diketone **22** was done via Grignard coupling of octylbromide with 1,3-dibromobenzene which was, upon lithiation and transmetalation with CuBr:LiBr, reacted with oxalyl chloride. Condensation of the final diketones **20** and **22** with their corresponding diamines results in the quinoxaline (**23,25,26**) and pyridopyrazine (**24**) monomers. The reaction yield for **24** is rather low, likely due to the deactivating nature of the imine nitrogen, presumably requiring longer reaction times or higher reaction temperature. The resulting monomers are copolymerized with bis(2,5-trimethylstannylthiophene) via Stille polymerization,^[89] to afford TQ1, TQ-8A, TQ-N and TQ-F in good yields.



Scheme 4.2: Synthetic route leading to TQ1, TQ-8A, TQ-N and TQ-F

4.2.2 Physical and optical properties

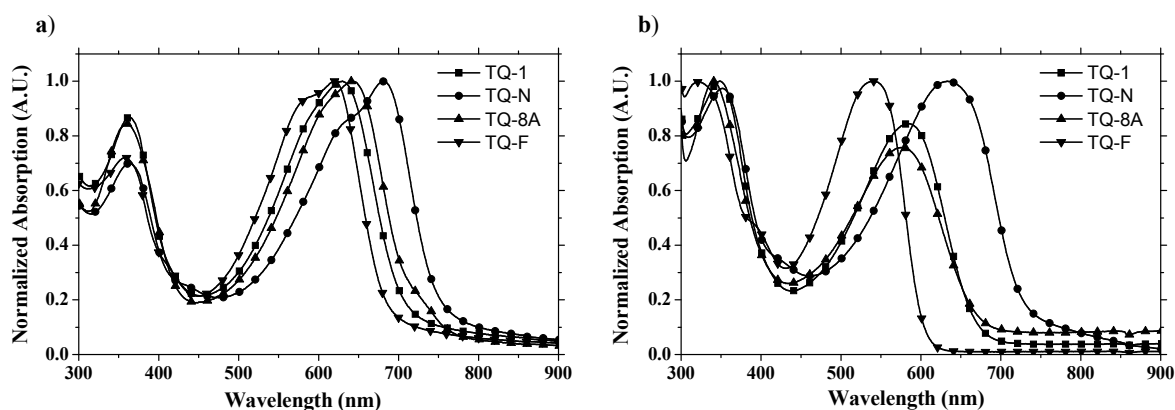
All polymers were obtained with reasonably high and similar number average molecular weights and high thermal stability (Table 4.2.1). Since the T_g for these polymers could not be recognized by differential scanning calorimetry (DSC), variable angle spectroscopic ellipsometry (Paper I, SI) was employed to determine thin film T_g on silicon substrates. The T_g of TQ-N and TQ-F was substantially lowered compared to the other two polymers which could originate from the induced changes in backbone structure, possibly due to irregularity (TQ-N) or due to increased dihedral angle (TQ-F).

Table 4.2.1: Physical properties of TQ derivatives

Polymer	M_n^a (kg mol^{-1})	PDI	TGA ^b ($^{\circ}\text{C}$)	T_g ($^{\circ}\text{C}$)
TQ1	46	2.6	370	100
TQ-N	35	5.1	420	46
TQ-8A	25	2.5	387	96
TQ-8A (2)	38	2.8	414	ND ^c
TQ-F	49	2.5	380	48

^a Measured against polystyrene standards in trichlorobenzene at 135 $^{\circ}\text{C}$. ^b 1% weight loss under N_2 atmosphere
^c Not determined

Solid state and solution UV-Vis absorption (Fig. 4.2.1) shows that the absorption of TQ-N is redshifted with about 40 nm compared to TQ1, and offers additional spectral coverage when combined with a fullerene derivative. Also, TQ-8A shows a small redshift in absorption. Even though TQ-F was designed with the intention to exhibit a similar absorption redshift as TQ-N, it instead shows a blueshifted absorption.

**Figure 4.2.1** UV-Vis absorption of the polymers in a) thin film and b) in hot DCB solution.

Square-Wave Voltammetry (SWV, Fig. 4.2.2) was used to estimate HOMO and LUMO levels and indicates that both the imine nitrogen and the fluorines are stronger acceptors. This is evidenced by the LUMO energy of TQ-N and TQ-F, which is shifted away from vacuum. Since TQ-F actually incorporates a stronger acceptor than TQ1, the blueshift in the UV-Vis absorption and the lower T_g is likely caused by an increased dihedral angle which would decrease orbital overlap. The HOMO energy is also shifted away from vacuum for both TQ-N and TQ-F which predicts a higher V_{oc} when these polymers are incorporated in photovoltaic devices. The slight redshift in the absorption of TQ-8A can be explained by the different electronic effect of the side chain on the energy levels of the polymer backbone, which is purely electron donating for an alkyl whereas an alkoxy sidechain combines this with a

resonance effect. Since the effect seems to be mostly on the HOMO, the V_{oc} would probably be somewhat reduced for TQ-8A based photovoltaic devices.

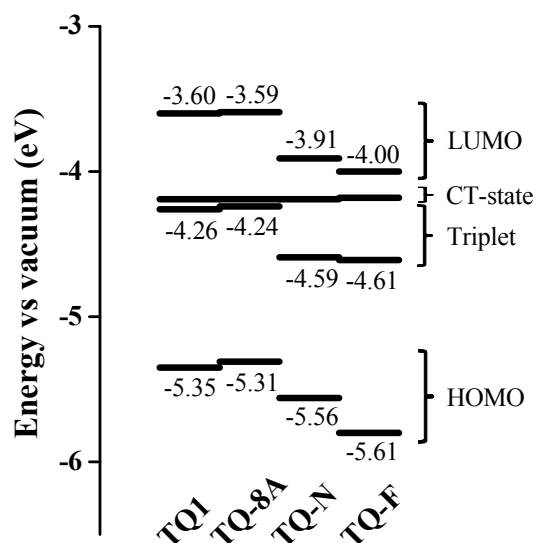


Figure 4.2.2 Energy diagram for each polymer in combination with PC₇₁BM. Optical (solid state) HOMO and LUMO energies were calculated from electrochemical E_{ox}/E_{red} onsets and the optical bandgap $E_{g, opt}$.

Table 4.2.2 Calculated energy values and energy offsets for $E_{g, opt}$, E_{CT} and E_T

Polymer	$E_{g, opt}$ (eV)	E_{CT} (eV)	$E_{CT} - E_{g, opt}$ (eV)	E_T (eV)	$E_T - E_{CT}$ (eV)
TQ1	1.75	1.16	-0.54	1.09	-0.07
TQ-N	1.65	1.37	-0.28	0.97	-0.40
TQ-8A	1.72	1.12	-0.58	1.07	-0.05
TQ-F	1.80	1.62	-0.08	1.19	-0.43
PC ₇₁ BM	1.70			1.40	

E_{CT} and E_T were calculated via the optical HOMO and LUMO energies of polymer and PC₇₁BM respectively. Details about these calculations can be found in paper 1 and ref 35

An experimental method was developed by Veldman *et al.* to relate energy offsets of the bandgap (E_g), CT-state (E_{CT}) and the triplet state (E_T) to various current-limiting mechanisms when using these polymers into BHJ-solar cells.^[35] It was derived that $E_g - E_{CT} > 0.08$ eV for efficient charge transfer and $E_{CT} - E_T < 0.1$ to suppress recombination of the CT-state via the triplet state. Particularly the energy difference between the CT-state and triplet state for TQ-N and TQ-F is large (Fig. and Table 4.2.2) so the probability for CT-to-triplet recombination would be increased for these materials. The $LUMO_{polymer} - LUMO_{PCBM}$ difference is reduced as well which is also indicated as a source for inefficient charge carrier generation.^[37] Arguably, in materials with too small $LUMO_{polymer} - LUMO_{PCBM}$ both loss mechanisms might well be present.

4.2.3 Photovoltaic performance

All polymers have been tested in combination with PC₆₁BM or PC₇₁BM as acceptor in photovoltaic devices (Table 4.2.3). In this study, TQ1 shows the best performance while the performance of TQ-8A is rather similar, with devices producing worse V_{oc} but better FF. TQ-F shows higher voltage due to a deeper HOMO but reduced current, its origin discussed in the

previous section. More interesting was the performance of TQ-N which showed, in contrast to what was estimated by electrochemistry, a strongly reduced voltage. A phenomenon that was thought to cause this problem was the acidity of PEDOT:PSS which, by protonation of the the TQ-N on the more accessible imine nitrogen potentially changes the workfunction or creates a charge collection barrier. This problem was circumvented by using molybdenum trioxide (MoO_3) which resulted in improved performance, most notably the V_{oc} .

Table 4.2.3 Photovoltaic data of devices based on polymer: $\text{PC}_{[x]}\text{BM}$ blends

Polymer	TQ: $\text{PC}_{[x]}\text{BM}$ (w:w)	$\text{PC}_{[x]}\text{BM}$	d (nm)	J_{sc}^a (mA cm^{-2})	V_{oc}^a (V)	FF ^a	η^a (%)	η^b (%)
TQ1	1:1	[61]	67	8.4	0.91	50	3.8	3.5 (0.22)
	1:1	[71]	84	9.6	0.89	49	4.2	3.4 (0.43)
TQ-8A	1:2	[71]	110	6.7	0.84	62	3.4	3.2 (0.14)
TQ-8A (2)	1:2	[61]	111	7.5	0.85	61	3.9	3.4 (0.24)
TQ-N	1:1	[61]	60	4.1	0.62	31	0.8	0.7 (0.07)
TQ-N ^c	1:1	[61]	100	4.5	0.97	27	1.2	1.1 (0.03)
TQ-F	1:2	[71]	61	3.4	0.99	50	1.6	1.5 (0.11)

ODCB as solvent, device architecture ITO/PEDOT:PSS/active layer/Yb/Al ^a Performance of the best cell. ^b Mean values and standard deviations, calculated from 8-15 devices. ^c MoO_3 as cathode instead of PEDOT:PSS

Aside from loss mechanisms due to imperfect energy level alignment, another factor that should be considered is the blend morphology. This is usually assessed by atomic force microscopy (AFM, Fig. 4.2.3) and, even though only the surface is scanned, some conclusions can be drawn. In the case of the four discussed polymers the morphology of all polymers, aside from TQ-N, seems rather similar. The combination of TQ-N and PCBM seems to result in a too intimately mixed blend morphology, possibly a result from favorable interactions between the free pyridine nitrogen and the fullerene,^[90] and is therefore possibly subjected to more severe loss mechanisms.

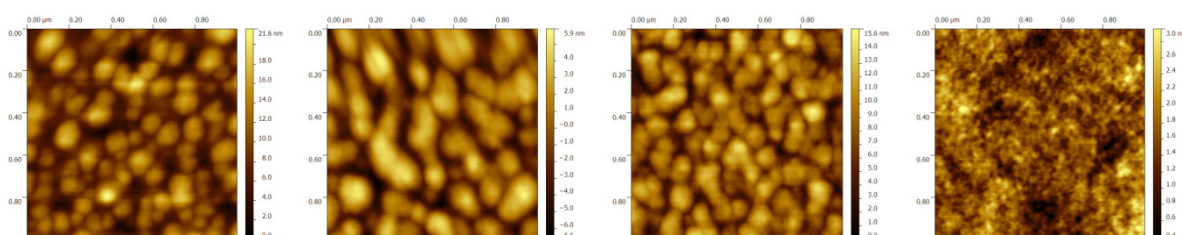


Figure 4.2.3 Topographical images from the in Table 4.3 indicated blends. From left to right, TQ1, TQ-8A, TQ-F and TQ-N, blended with $\text{PC}_{[x]}\text{BM}$. The AFM image length scale is $1 \times 1 \mu\text{m}$.

4.3 Side chain modifications on TQ1

A continuation of the work (**paper II**) describes how the alternating quinoxaline-thiophene backbone was retained but instead, the pendent alkoxyphenyl side group was substituted with alkylthiophene. By substituting the alkoxyphenyl with the more electron-donating alkylthiophene, the bandgap of the quinoxaline-based acceptor was reduced. It is possible to consider the resulting material as a DAD segment, where the D-A interaction between the quinoxaline acceptor and the pendent thiophene is stronger than in TQ1, which incorporates a much weaker interacting ‘phenyl donor’. Additionally, the electron donating thiophene shifts the HOMO of the quinoxaline-thiophene towards vacuum. By incorporating an accepting unit that has a smaller bandgap with both HOMO and LUMO levels inside the energy levels of the backbone thiophene, it is the acceptor in this case that mainly determines the bandgap (density functional theory (DFT) calculations). In combination with the delocalization gained along the polymer backbone the resulting polymer (**TQ-T8**) displays a smaller bandgap than TQ1, but also a HOMO which is shifted towards vacuum.

To mitigate the electron donating effect of the thiophene and combine a redshifted absorption with a deep HOMO level thereby potentially maximizing V_{oc} , three different electron withdrawing groups have been added adjacent to the thiophene; carbonyl, difluoromethyl and –ylidene malononitril.

4.3.1 Synthesis

The synthetic route is depicted in scheme 4.3. Friedel-Crafts acylation of thiophene with octanoyl chloride results in compound **27**. The carbonyl is subsequently protected by conversion of the carbonyl to an acetal group (**28**). Then lithiation, transmetallation and coupling with oxalyl chloride yields diketone **29** which is condensed with 3,6-dibromobenzene-1,2-diamine (**30**) (compound **13**, chapter 4.2.1) and subsequently deprotected to offer monomer **31**. The difluoromethylene group (**32**) and the ylidene malononitril group (**32**) could conveniently be obtained by transforming the carbonyl side group on the monomer via Knoevenagel condensation or Deoxofluorination (Scheme 2). It seems that the electron donating thiophene deactivates the carbonyl somewhat, since conventional reaction conditions for Knoevenagel condensation (malononitril (active hydrogen compound) + pyridine (base)) resulted in the starting material. Therefore, Lehnerts’ reagent was used to activate the carbonyl which resulted in the target compound.^[91] Rather harsh conditions also had to be employed to introduce the difluoromethyl group, possibly a

backbone planarity, either due to the meta versus more para-like orientation of the side chains or due to less steric interaction between the thiophene side groups in solid state. In the case of TQ-T8(CF₂)₂ this effect seems to be reduced which was attributed to a ‘kink’ induced by the Gauche effect that, due to steric hindrance between the polymer chains, prevents aggregation and result in a higher molecular weight.

Table 4.3: Physical and optical properties of the polymers

Polymer	M_n^a (kg mol ⁻¹)	PDI	TGA ^b (°C)	Abs _{onset} ^c (nm)	$E_{g, calc}$ (eV)	$E_{g, ec}^d$ (eV)	$E_{g, opt}^d$ (eV)	$\epsilon_{low}/10^4$ ^e (L*mol ⁻¹ *cm ⁻¹)	$\epsilon_{high}/10^4$ ^e
TQ-T8	17	5.5	470	749	2.16	1.86	1.66	1.86	3.02
TQ-T8(CO) ₂	18	2.4	452	780	1.92	1.77	1.59	1.87	3.56
TQ-T8(CF ₂) ₂	44	3.1	416	806	2.05	1.78	1.54	1.53	2.18
TQ-T8(Mal) ₂	8	1.7	403	860	1.40	1.53	1.44	1.20	5.78

^a: Measured against polystyrene standards in trichlorobenzene at 135 °C, ^b: N₂ atmosphere, 5% weight loss, ^c: thin film absorption, ^d: from peak onsets, ^e: calculated via the repeating dimer mass

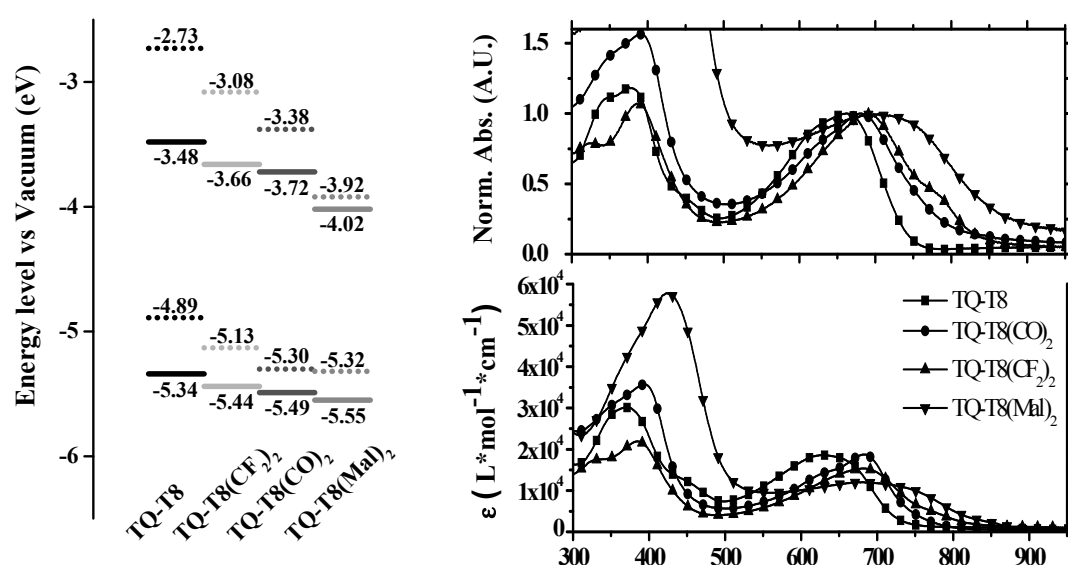


Figure 4.3 a) HOMO and LUMO levels calculated from electrochemistry (solid lines, via $-(E_{red/ox} + 5.13)$ and DFT-calculations (dotted lines, PW91/DNP(basis file 4.4) with Dmol³ program package), b) top, UV-Vis absorption in solid state, normalized on the low energy absorption peak; bottom, solution absorption in chloroform, normalized on chromophore concentration (avg. of 3 measurements).

The combined results from electrochemistry, DFT calculations and UV-Vis absorption spectroscopy indicate that the electron donating nature of the pendent thiophene can be mitigated (Fig 4.3a), even by the long range effect of electron withdrawing side groups. For all side chain modifications both a deeper HOMO and a redshifted absorption is obtained (Fig 4.3b), which are beneficial properties for the use in solar cell materials. At least for TQ-T8 it

seems that the energy levels aren't simply governed by what is usually designated as donor-acceptor interaction but more by the energy levels of the acceptor. In combination with backbone delocalization it results in the energy levels of the respective polymers.

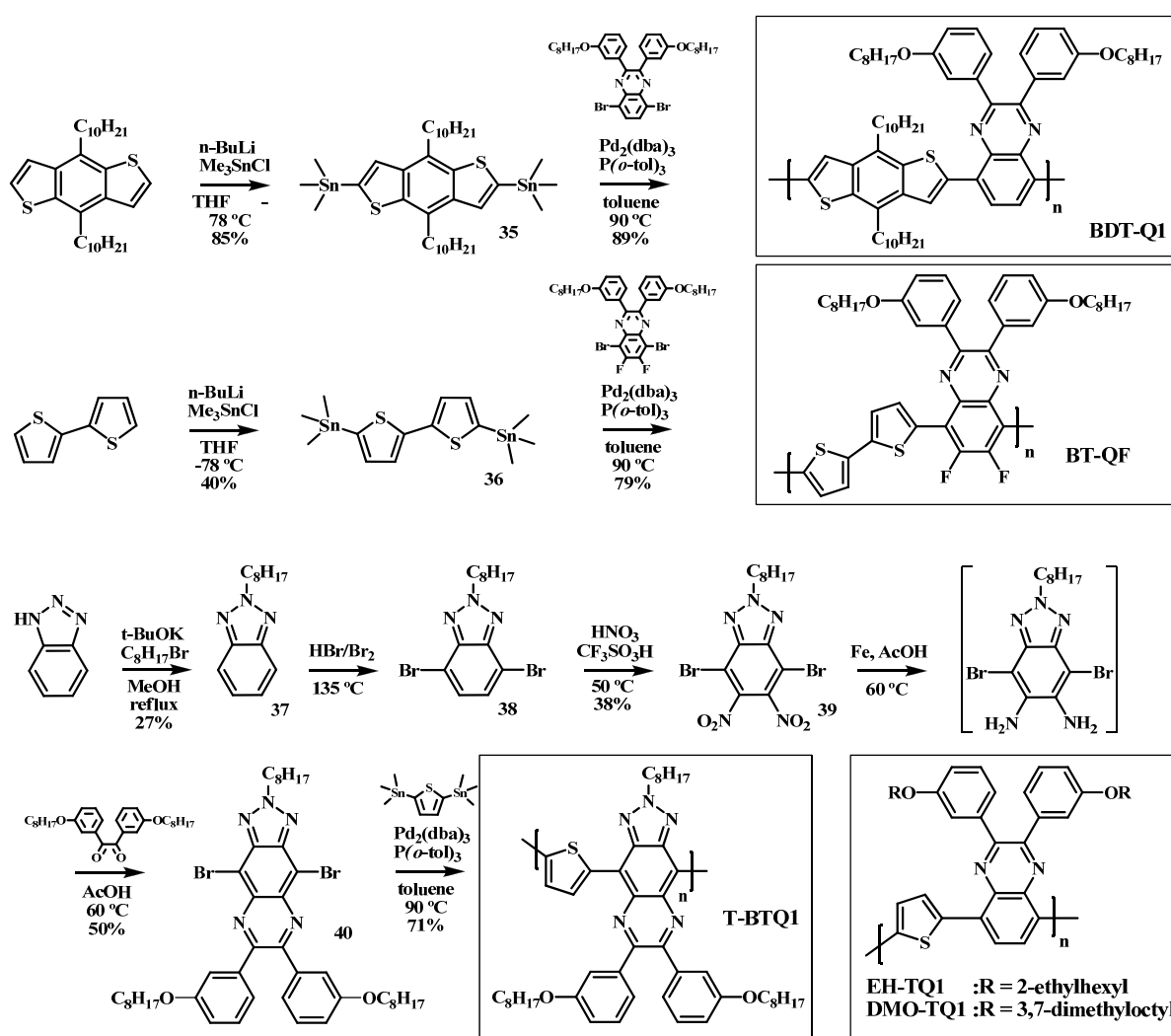
4.4 Other TQ1 related polymers

Some other polymers (Scheme 4.4) have been synthesized based on either the backbone structure of TQ1 or the 2,3-bis(3-(octyloxy)phenyl)quinoxaline acceptor unit. Two polymers, **EH-TQ1** and **DMO-TQ1**, have identical backbone structures as TQ1 but incorporate branched 2-ethylhexyloxy and 3,7-dimethyloctyloxy side chain, initially to improve solubility and molecular weight since higher molecular weight generally improves the efficiency of polymer solar cells.^[92, 93] Three other polymers have also been synthesized which either incorporate different donors or acceptors. In one polymer (**BDT-Q1**) the thiophene donor was replaced with a benzodithiophene (BDT) donor, a fused unit that potentially improves π - π stacking in the material, thereby improving mobility^[94] and active layer thickness in solar cells.^[95] A second material (**BT-QF**) was synthesized based on the 6,7-difluoro-2,3-bis(3-(octyloxy)phenyl)quinoxaline monomer and bithiophene (BT). Since the addition of fluorine increases the dihedral angle in the polymer backbone, it would be possible to still obtain a soluble material with a more planar backbone by adding an additional thiophene spacer. Also, since additional donor units are added in the backbone, the HOMO would shift towards vacuum and induce an absorption redshift compared to TQ1. A third polymer incorporates a combination of 2,3-bis(3-(octyloxy)phenyl)quinoxaline and a triazole ring which offers a rather strong acceptor. This acceptor was polymerized with thiophene to afford a small bandgap polymer, **T-BTQ1**.

4.4.1 Synthesis

Introduction of the branched side chains in EH-TQ1 and DMO-TQ1 is similar to TQ1 (Scheme 4.1) with the exception that 2-ethylhexyl- and 3,7-dimethyloctylbromide is used during the Williamson ether synthesis when synthesizing compound **20**. The synthetic scheme leading to BDT-Q1, BT-QF and T-BTQ1 is depicted in Scheme 4.4. Lithiation of didecylbenzodithiophene or bithiophene and subsequent reaction with trimethylstannylchloride resulted in the stannylated monomers **35** + **36**. The synthesis of the distannyl-BDT unit **35** was performed with a 3-fold excess of n-BuLi and Me₃SnCl since the

usual stoichiometric ratios (typically 2.1-2.2 fold excess of n-BuLi) resulted in a mixture of mono and distannylated material. In the synthesis of benzotriazole **37**, the reaction yield is rather low which could be the result of using a protic solvent (MeOH).^[96] DMF as the solvent was reported to result in higher reaction yields. Subsequent nitration (**38**), reduction and condensation with **20** offers the strong acceptor **40**. Again, the stannylated and dibrominated monomers were polymerized using Stille coupling which results in BDT-Q1, BT-QF, T-BTQ1, EH-TQ1, DMO-TQ1. During the Soxhlet purification step BDT-Q1 was extracted completely in diethyl ether, a solvent normally considered to be a non-solvent for these conjugated polymers.



Scheme 4.4 synthetic scheme leading to PBDT-Q1, PBT-QF and PT-BTQ1 and the structures of EH-TQ1 and DMO-TQ1. $C_{10}\text{BDT}$ unit was generously donated by Merck.

4.4.2 Physical and optical properties

The obtained polymers all exhibit decent molecular weights (Table 4.4.1), but BT-QF and T-BTQ1 have rather high PDI. For BT-QF this was ascribed to solubility issues since the SEC-trace showed a ‘trimodal’ distribution, which is likely a result from increased backbone planarity resulting in aggregation. In case of T-BTQ1 the SEC-trace showed a bell-shaped curve but a rather long tail at shorter elution times. EH-TQ1 and DMO-TQ1 show much lower molecular weight compared to TQ1 which was opposite from expected.

Table 4.4.1 molecular weight, optical and redox properties of the polymers

Polymer	M_n^a (kg mol^{-1})	PDI	$E_{g, \text{opt}}^b$ (eV)	HOMO ^c (eV)	LUMO ^c (eV)	$E_{g, \text{ec}}$
BDT-Q1	20	2.2	1.79	-5.39	-3.53	1.86
BT-QF	20	22.5	1.63	-5.27	-3.51	1.76
T-BTQ1	39	8.8	1.19	-5.34	-3.92	1.42
TQ-F	49	2.5	1.80	-6.04	-3.76	2.28
TQ1	46	2.6	1.75	-5.50	-3.44	2.06
EH-TQ1	15	2.2	1.72	-5.50	-3.58	1.92
^d DMO-TQ1	22/25	2.6/2.3	1.74	-5.33	-3.53	1.80

^a Measured against polystyrene standards in trichlorobenzene at 135 °C, ^b calculated via absorption onset, ^c calculated via oxidation or reduction peak onset, $-(E_{\text{red/ox}} + 5.13)$, ^d two synthesized batches

Electrochemistry (Table 4.4.1) shows that, compared to TQ1, all polymers display similar HOMO levels that are shifted towards vacuum which theoretically indicates similar but reduced V_{oc} for all materials. The LUMO of BDT-Q1 and BT-QF are also rather similar to TQ1 but T-BTQ1 has a drastically lowered LUMO level due to the strong acceptor nature of the BTQ1 unit. Interestingly, even though TQ-F (chapter 4.1) displays a deep HOMO level it seems to be largely counteracted (HOMO towards vacuum) by the addition of an additional thiophene, which concomitantly shifts the HOMO level towards vacuum and planarizes the backbone of BT-QF. The different side chains in EH-TQ1 and DMO-TQ1 do not seem to significantly influence the energy levels of the TQ1 backbone.

A possible explanation for the reduced molecular weight of EH-TQ1 and DMO-TQ1 compared to TQ1 can be found in the UV-Vis absorption (Fig 4.4a). A small redshift and an increasing shoulder peak can be recognized for $\text{TQ1} < \text{DMO-TQ1} < \text{EH-TQ1}$, which, combined with the reduced molecular weights, indicates an increased tendency to aggregate, likely resulting from reduced steric hindrance. The same effect can actually be seen for TQ-8A, where the low energy UV-Vis absorption shows a similar shoulder peak as DMO-TQ1. It

would suggest that not only the effect of the branched side chains on steric hindrance is of importance, but also that the ether bond affects this.

The UV-Vis absorption onset of TQ1, TQ-F and BDT-Q1 is rather similar (Fig. 4.4b), except for the depression between the high and low energy absorption peak which is partly filled for BDT-Q1. This is probably caused by the extended aromatic structure of BDT which would absorb in this region. The absorption of BT-QF is shifted about 80 nm into the near IR and broadened when compared to TQ1/TQ-F, which is convenient when attempting to absorb more photons. The strong electron accepting nature of the T-BTQ1 unit (**40**) causes the absorption to be redshifted well into the near-IR region.

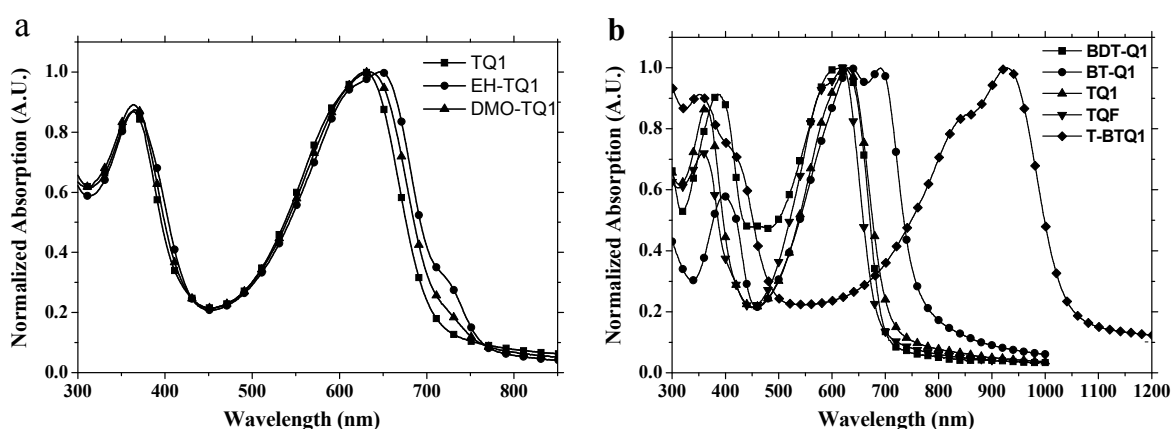


Figure 4.4 solid state absorption of a) EH-TQ1 and DMO-TQ1 compared with TQ1 and b) BDT-Q1, BT-QF and T-BTQ1 compared with TQ1 and TQ-F

4.4.3 Photovoltaic performance

Table 4.4.2 Photovoltaic performance (best cells, not optimized) of devices based on polymer: PC_[x]BM blends

Polymer	TQ: PC _[x] BM (w:w)	PC _[x] BM	d (nm)	J_{sc} (mA cm ⁻²)	V_{oc} (V)	FF	η (%)
BDT-Q1	1:1	[61]	50-60	3.7	0.88	55	1.8
BT-QF	1:2	[71]	71	4.8	0.73	55	1.9
T-BTQ1	1:1	[71]	56	2.2	0.54	36	0.4
EH-TQ1	1:1	[61]	50-60	2.2	0.89	48	0.9
DMO-TQ1	1:1	[61]	50-60	2.8	0.88	42	1.0

ODCB as solvent, device architecture ITO/PEDOT:PSS/active layer/Yb/Al

All polymers were tested on their photovoltaic performance in combination with a fullerene derivative (Table 4.4.2). Rather high V_{oc} could be obtained for all polymers except

for T-BTQ1, which offers smaller V_{oc} . Current densities and FF are low for T-BTQ1, which cannot be explained properly without additional investigation, but likely reasons are the small $LUMO_{polymer}-LUMO_{PCBM}$ difference and blend morphology. BDT-Q1 and BT-QF show moderate J_{sc} and decent FF, which results in a PCE of 1.8-1.9% in this study. When comparing EH-TQ1 and DMO-TQ1, mainly the current density is decreased compared to TQ1, possibly by an unfavorable morphology.

4.5 TQ1 derivatives in electrochromics

Most studies that involve TQ1 focus on its properties in BHJ-solar cells and include synthesis and photovoltaic performance, blend morphology and environmental stability.^[97, 98] As conjugated polymers exhibit useful properties such as solution processability, low oxidation potentials, fast response times and color tunability, they are promising materials for applications such as smart windows, e-papers and low-cost displays. Therefore, TQ1 also has been tested on its electrochromic properties and additionally, a study was done to establish structure-property relationships as function of side chain modifications (**paper III**).

4.5.1 Physical and opto-electronic properties

One TQ1 derivative that was used in this study was EH-TQ1 (in paper III designated TQ3). As mentioned before, a lower molecular weight (Table 5.4) combined with a shoulder peak and more pronounced vibronic features in the low energy peak absorption (Fig 4.5.1) suggests that EH-TQ1 exhibits improved solid state ordering.

Table 4.5 Molecular weight and redox properties of TQ1 and TQ-EH

Polymer	M_n ($kg\ mol^{-1}$)	PDI	E_{ox}^a (eV)	E_{red}^a (eV)
TQ1 ^b	56	3.0	0.43	-1.62
EH-TQ1	15	2.2	0.43	-1.55

^a E_{ox} and E_{red} determined vs F_c/F_c^+ ^b a different TQ1-batch was used for this study

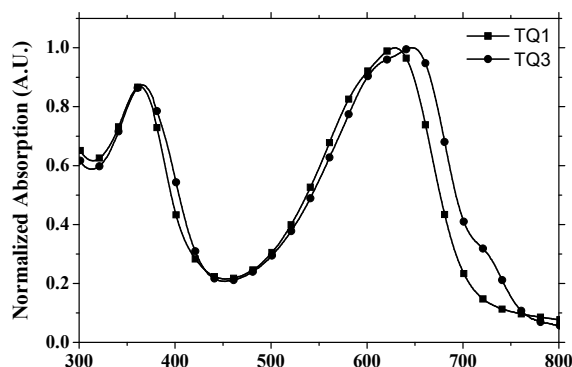


Figure 4.5.1 UV-Vis absorption of polymers in thin film

When comparing optical contrast and switching times (Fig. 4.5.2 a + b), TQ1 performs slightly better, while TQ3 has better response at faster switching speeds. Two reasons could explain this; the ethylhexyloxy sidechain would increase the interchain distance, or reduced solubility in combination with a fast drying solvent during spraycoating (CHCl_3) would cause a more open thin film morphology which then facilitates ion transport during oxidation.

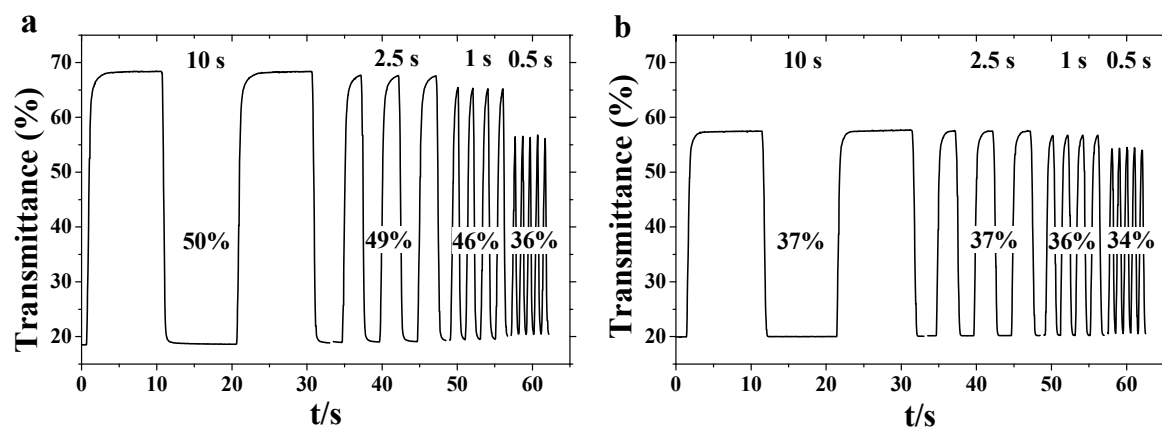


Figure 4.5.2 Kinetic measurements on TQ1 (a) and EH-TQ1 (b) films on ITO, using 0.1 M NBu₄PF₆ in anhydrous acetonitrile as supporting electrolyte. Films were switched between 0 and +1.0 V.

Chapter 5

DIKETOPYRROLOPYRROLE-BASED POLYMERS

5.1 Introduction

Another type of acceptor that has been often incorporated in conjugated polymers is the diketopyrrolopyrrole (DPP) unit. DPP has its origin as a strongly colored dye, where the most famous one is ‘Red Pigment 254’ (Fig 5.1), or more commonly ‘Ferrari Red’.

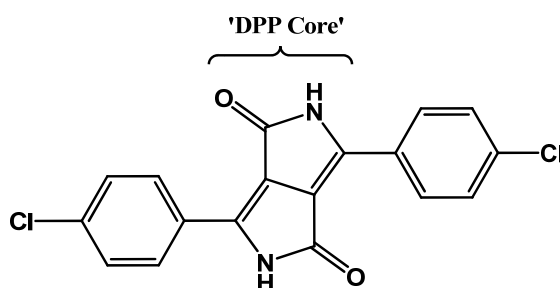


Figure 5.1 chemical structure of ‘Red Pigment 254’

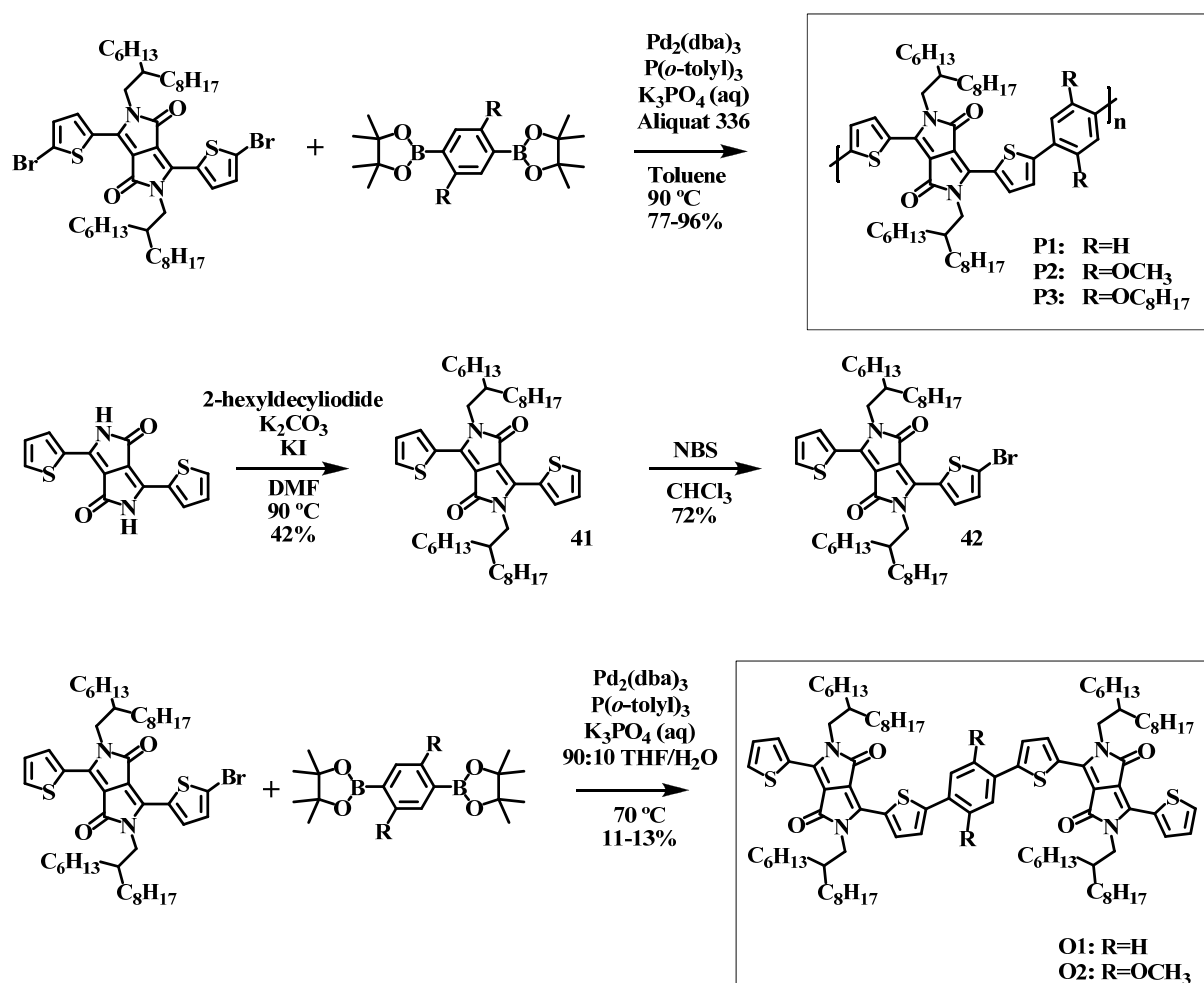
The DPP core is usually formed by condensation between an aryl-carbonitril and diethylsuccinate, which results in the DPP core always being flanked by two aromatic units.^[99] The resulting DPP unit is virtually planar, e.g. the phenyl side groups display 7° dihedral angle, which facilitates π - π interaction between oligomers and polymers.^[100] It is convenient to use thiophene-based donors for the formation of the DPP-unit since it results in an absorption redshift of the optical absorption. Polymers based on this acceptor unit offer among the highest performances in BHJ-solar cells.^[19, 101]

Bijleveld *et al.* recently reported a copolymer based on 2,5-bis(2-hexyldecyl)-3,6-di(thiophen-2-yl)pyrrolo[3,4-c]pyrrole-1,4(2H,5H)-dione and benzene (scheme 5). Photovoltaic devices based on a blend of the so-called PDPPTPT (hereafter designated as P1) and PC₇₁BM reached good power conversion efficiency of 5.5% after optimization with a processing agent.^[102] The addition of alkoxy side chains on the phenyl spacer allowed for a redshifted optical absorption and a shift of the HOMO level towards vacuum. In an attempt to ascertain structure-property relationships more specifically, P1 was modified with methoxy and octyloxy side chains. The effect of adding methoxy and octyloxy side chains to the benzene spacer on various polymer properties has been investigated. Well-defined oligomers

were also synthesized and characterized to verify some structure-property relationships. (paper IV).

5.2 Synthesis

The polymers (Scheme 5.1) were synthesized via Suzuki cross-coupling and were obtained in high yields. Compound **41** was obtained after N-alkylation which was brominated with NBS to offer the monobrominated material **42**. The Suzuki conditions used for the DPP-oligomers synthesis proved to be too harsh, resulting in a translucent red solution instead of the expected deep blue/purple colored solution which seemed to be a result of degradation. Switching to milder reaction conditions results in formation of the desired product although the debrominated and homocoupled product was also identified by matrix-assisted laser desorption/ionization time-of-flight (MALDI-TOF).



Scheme 5.1 Synthetic route leading to DPP-based polymers and oligomers.

5.3 Physical and optical properties

All polymers were obtained with reasonable molecular weight where the solubilizing octyloxy side chains on P3 improve solubility and therefore molecular weight.

TGA (Table 5.1) indicates that the thermal stability is somewhat decreased upon addition of the alkoxy side chain. Melting and crystallization temperatures, determined by DSC (Table 5.1) are reduced more with increasing alkoxy side chain length which is consistent with having additional movement in the polymer chain. This trend is however not reflected in the oligomers, where the methoxy substituted oligomer (O2) shows higher T_m and T_c than the unsubstituted oligomer (O1), but the origin of this effect needs to be investigated further. The difference in T_m/T_c evolution between oligomers and polymers could be ascribed to an incomplete representation of P1 and P2 by O1 and O2 since additional alkoxyphenyl-based units would increase backbone irregularity.

X-ray diffraction (manuscript IV, SI) indicates that all polymers exhibit significant ordering. The longest range order is found for P1, then P2 and finally P3.

Table 5.1 : physical properties of oligomers and polymers

Material	M_n (kg/mole) ^a	PDI	TGA (°C) ^b	T_m ^c	T_c ^c	HOMO ^d	LUMO ^e
			1% wt. loss	(°C)	(°C)	(eV)	(eV)
P1	15	1.5	415	>350	>350	-5.10	-3.58
P2	12	2.7	336	>300	260	-4.89	-3.55
P3	29	2.3	347	240	190	-4.88	-3.56
O1	-	-	257	153	110		
O2	-	-	341	181	148		

^aMeasured against polystyrene standard in TCB at 135 °C, ^b under nitrogen atmosphere, 1% weight loss, ^c determined from the 2nd heating scan, via LUMO – $E_{g,opt}$ ^e calculated via oxidation or reduction peak onset, – ($E_{red} + 5.13$)

The optical absorption (Fig 5.1a+b) has been redshifted towards the NIR due to the electron donating side chains that shift the HOMO towards vacuum (Table 5.1), but also predicts lower voltage for BHJ solar cells based on P2 and P3. The broadening of the UV-Vis absorption due to alkoxy substitution could be caused by the increased flexibility in the polymer chains which then increases the conformational distribution. P1 seems to absorb stronger in solution (Fig 5.1a), which could be attributed to the stiffer backbone which either promotes intrachain aggregation or a more rod-like behavior which then decreases the conformational distribution in the polymer chain and therefore a less broad absorption.

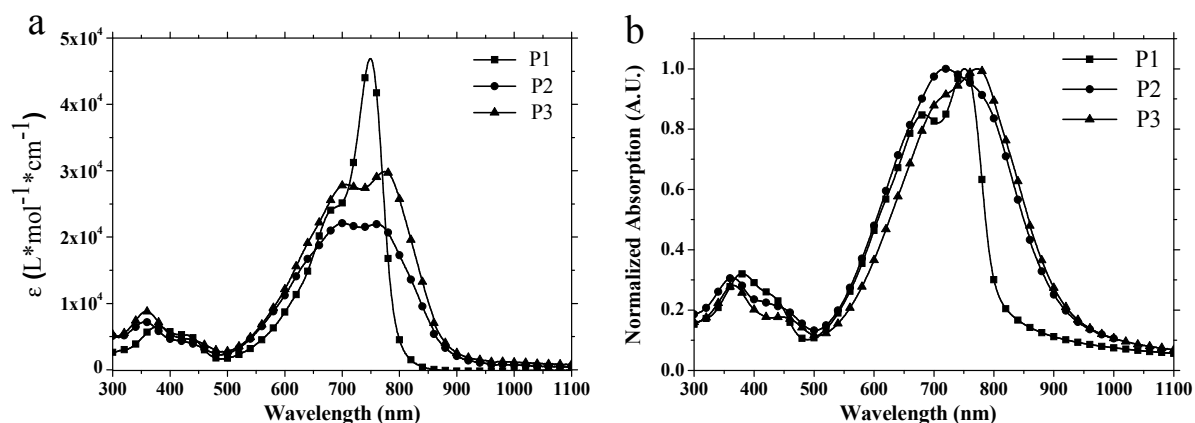


Figure 5.1: UV-Vis absorption of (a) dilute polymer solutions (CHCl_3 , $\sim 16 \text{ mg L}^{-1}$) and (b) solid state, spun from $\sim 10 \text{ mg mL}^{-1}$ CHCl_3 solutions.

UV-Vis solution measurements of dilute polymer solutions in 1-chloronaphthalene indicate that P1 exhibits the lowest solubility, followed by P2 and then P3 (manuscript IV, SI). The DSC, X-ray diffraction and solubility measurements seem to agree with each other rather well, which indicates that the modifications done on the parent structure result in additional flexibility of the polymer chain. This will likely affect the final blend morphology and performance when these polymers are tested in BHJ solar cells.

5.4 Photovoltaic performance

All polymer BHJ solar cells were constructed with PC_{71}BM as the acceptor (Table 5.2) and 1,8-diiodooctane (DIO) as the cosolvent. Comparing the PV-performance of polymer: PC_{71}BM BHJ solar cells, the voltage of both P2 and P3 based devices are limited. This is likely caused by the reduction of $\text{HOMO}_{\text{donor}}\text{-LUMO}_{\text{acceptor}}$ due to the electron donating effect of the alkoxy side chains. Particularly the optical response in the 600-800 nm region is much lower when comparing P3 to P1 based devices (Fig. 5.2b), but still a decent current is obtained for P3.

Table 5.2: Photovoltaic data of devices based on polymer: PC_{71}BM blends

Material	Polymer: PC_{71}BM (w:w)	Thickness (nm)	RMS blend (nm)	J_{SC} (mAcm^{-2})	V_{OC} (V)	FF	η (%)
P1	1:2	125	2.77	8.4	0.78	49	3.2
P2	1:2	80	10.9	3.4	0.59	45	0.9
P3	1:2	77	4.27	7.1	0.60	46	2.0

Active layers spun from 5-15 mg mL^{-1} polymer: CHCl_3 with 23 mg mL^{-1} DIO. Device architecture ITO/PEDOT:PSS/active layer/Yb/Al

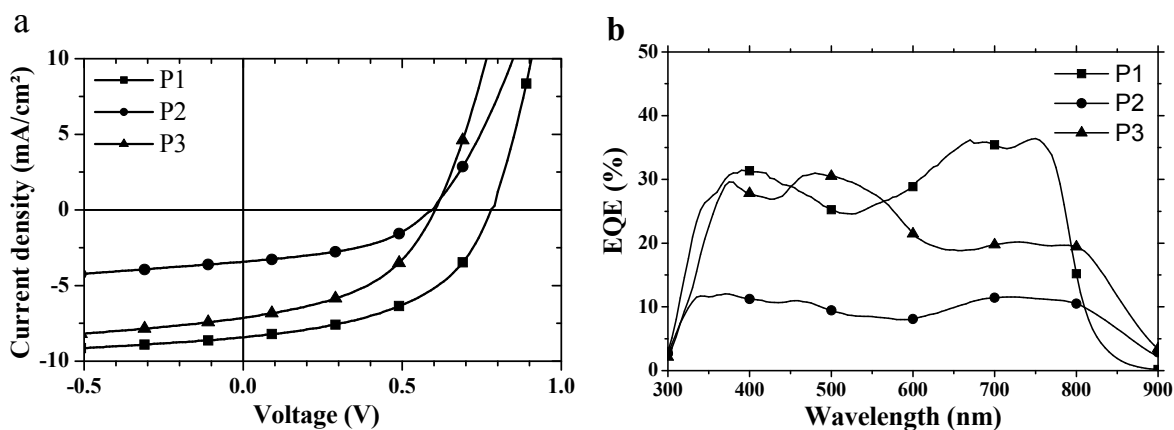


Figure 5.2 IV-curve (a) and EQE (b) for polymer:PC₇₁BM BHJ solar cells

A possible explanation for the lower current of P2-based solar cells can be found via AFM (Fig 5.3), which shows increased surface roughness and a distinctly different morphology compared to the other two polymers.

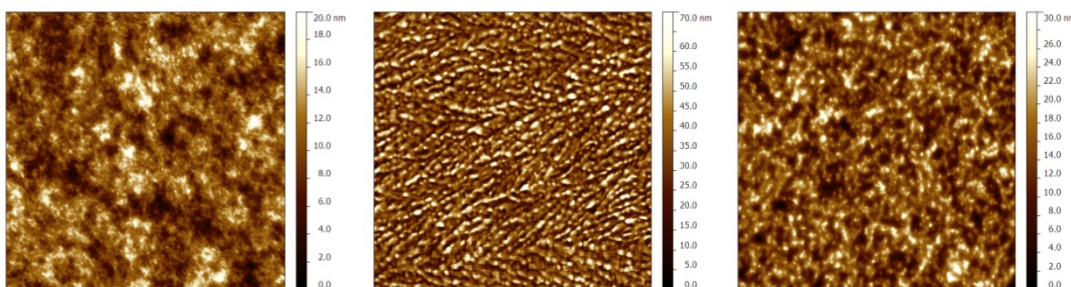


Figure 5.3, AFM topographical images (5x5 μm) for the P1, P2 and P3:PC₇₁BM blends respectively

5.5 PDPPTPT as donor polymer in hybrid solar cells

Aside from being utilized as an efficient polymer donor material in polymer:fullerene BHJ solar cells, PDPPTPT was also used as the donor material in hybrid solar cells. Among the materials that can be utilized for colloidal inorganic nanocrystals (NCs); CdSe, CdTe, PbSe, CdS, lead sulfide (PbS) stands out because of high mobility, broad absorption and air stability. Combining polymers with this inorganic acceptor imposes certain criteria such as a suitable energy level alignment, choice/exchange of ligand molecules and morphology, in order to result in high PCE for hybrid solar cells. Because fundamental understanding of such systems in solar cell configuration is still limited, charge carrier dynamics of PDPPTPT:PbS BHJ solar cells were investigated to provide deeper insight in the working principle of this system (paper V).

Devices were fabricated by spincoating chloroform solutions of PDPPTPT:PbS and oleic acid (OA) on ITO substrates after which a ligand exchange of OA for 1,4-benzenedithiol was performed. Successive spincoating and ligand exchange (15-18 times) resulted in uniform, crack-free active layers (thickness 110-120 nm), which displayed a broad spectral coverage starting from 1400 nm. The best device displayed $J_{sc} = 12.5 \text{ mA cm}^{-2}$, $V_{oc} = 0.47 \text{ V}$, $FF = 49\%$ and PCE of 2.9%.

Comparison of charge carrier dynamics against a PDPPTPT:PC₆₁BM BHJ indicates efficient charge transfer for both systems, which is somewhat surprising for the hybrid solar cells due to the very small $\text{HOMO}_{\text{polymer}}\text{-HOMO}_{\text{PbS}}$ offset. Different suggestions for the limited performances were made; for the PDPPTPT:PCBM solar cells an unoptimized blend morphology while for the hybrid solar cells defects at the polymer:Pbs nanocrystal interface and traps were suggested as loss factors.

Chapter 6

CONCLUDING REMARKS

The work in this thesis focused on both maximizing opto-electronic properties of p-type polymers for polymer:fullerene BHJ solar cells and on how structure-property relationships are influenced upon structural modification of a parent structure.

Chapter 3 showed that substituting a carbon for a silicon bridging atom imposes a very subtle influence on the optical, electrochemical and photovoltaic properties while the influence on the thermal properties is still surprisingly large. One promising parameter to investigate in the future would be the influence of backbone curvature on the properties of these polymers.

Chapter 4 demonstrated the vast possibilities to adjust energy levels and bandgap energies of TQ1, whether this is via structural modification of the polymer backbone or via side chain modifications. Several additional effects have been found that alter physical, optical and photovoltaic properties which include protonation, steric effects due to atom size or side chain length, or the Gauche effect.

Alkoxy substitution on the parent PDPPTPT polymer (chapter 5) influenced various polymer properties, consistent with increased flexibility in the polymer chains. By comparing oligomer and polymer properties it seems though that alkoxy substitution initially increased T_m and T_c . Arguably, this effect is then counteracted by increased backbone irregularity of the polymer which would increase the conformational entropy. An increased HOMO level for the alkoxy-substituted polymers and altered blend morphology seem to limit the photovoltaic performance of the alkoxy substituted polymers, while PDPPTPT shows good efficiencies not only combined with PB₇₁BM, but also with inorganic PbS nanocrystals as acceptor.

As a final conclusion to this work, every structural change induces one or more additional alterations in polymer properties with sometimes unexpected results. Some effects can result from interactions between different compounds while other effects can result from electronic interactions between donor and acceptor units, bond length differences or other unforeseen effects. Since the research field in organic electronics is maturing, it will be increasingly important to consider as many factors as possible in order to map the full impact of a structural modification done on a polymer relative to the efficiency of a photovoltaic device.

ACKNOWLEDGEMENTS

I would like to thank the following people for the way I have experienced my Ph.D.; an educative, sometimes stressful but most of all a very fun and entertaining period.

Mats R. Andersson, for accepting me four-and-a-half years ago as a Ph.D. student in organic electronics and sharing your knowledge. I included the important ‘R.’, but what a problems it causes when submitting papers...

Christian Müller, for being a very knowledgeable, inspiring and encouraging person.

Tim Steckler, for being intimately involved in teaching me the tricks of the trade regarding organic synthesis. Agi Stépan, for being a fantastic office mate and my own private in-house connection to Holland. Tina Gschneidtner, for always taking the initiative in doing something fun. All three of you are great friends and I will never forget the good times we had, especially in Åbisko!

Hanne Evenbratt, for being a fun person to talk to and for the ‘skjuss hem’. It is surprising that there exists another person as chaotic and blurry at times as I am. Annika Borde, for letting me win all the time with badminton ;), and for the leg-up you gave me during writing this thesis.

Christina Meyer, Anne Wendel, Ann Jacobson, Carina Pettersson, Maria Wåhlin, Frida Andersson, Anders Mårtensson and Roger Forsberg for EVERYTHING that is involved in enabling the daily life and traditions at our department. Anders is additionally acknowledged for all SEC measurements.

The people from our organic electronics group; Stefan Hellström and Patrik Henriksson, for all the electrochemistry. Desta Gedafaw and Wendimagegn Mammo, for guidance in the beginning of my Ph.D. and for the crash-course in Amharik. Egzhiabher Yimesgen! Ergang Wang, for valuable input during my Ph.D. period. Zandra George and Camilla Lindqvist, for sharing some projects and a several wonderful conference trips, Angelica Lundin for all those DFT-calculations and discussions about orbitals, Wenliu Zuang, for your input, especially regarding my latest project. It is time for your cake-baking exam! Sandra Fusco, for being the best tourguide during project meetings ever. Lars Lindgren, Markus Jarvid, Mattias Andersson, Zelalem Abdissa and our newest addition Amaia Diaz de Zerio, simply for good times.

The incredible amount of nice and funny master students I got to know. Each of you has something special and I simply cannot put this on paper since it will make my thesis twice as thick, but thank you for choosing floor 8 as your place to graduate.

All the other colleagues I have/had in my years at the department, Sven Engström, Villgot Englund, Annette Larsson, Anders Höije, Karin Sterky, Susanne Nilsson, Linus Karlsson, Kristian Thörnblom, Pernilla Karmalm, Magnus Svensson, Anna Viridén, Anna Bergstrand, Anna Ström, Sofie Gårdebjer, Helene Andersson, Anders Johnson, Wolo, Arne Holmström, Mikeal Larsson, Johanna Eckardt, Anders Lennartsson, Karl Börjesson, Yuri Diaz Fernandez, Kasper Moth-Poulsen and Guillermo Toriz Gonzalez (Mr. Dry Ice). Together with all the people mentioned before, thank you for contributing to the working atmosphere at Floor 8!

The people involved in the collaborations over the years, especially Robert Gehlhaar and Afshin Hadipour from IMEC who performed the photovoltaic characterization of my materials, and Annemarije Andringa, for sharing the ONE-P experience with a bunch of Swedish organic chemists.

A special thanks goes to Lilian and Ragnar, which are friends disguised as our landlords. Thank you for taking us in above the stable, for all the commuting, dinners and many more things. We found a great home in Hindås and we are very grateful.

My friends back home, for reminding me of all we still have in the Netherlands.

Even though I haven't seen them so much in the past years, my brothers Mark and Edwin, their better halves Trienke and Marina, my grandpa and grandma, my parents-in-law Tineke and Jaring, my sister-in-law Nadine and Rik and the rest of my family.

My dad Henk and my mom Carla, for all their love and care and in guiding me to where I am right now.

Liona, sometimes I am a disaster to live with and I know it. Even though you are definitely not into chemistry, I'm quite sure my best experiment is with you (maybe I'll regret it after the first week of 0% sleep and 100% dippers). I love you very much.

REFERENCES

1. BP Statistical Review of World Energy, in June 2012.
2. IEA, *World Energy Outlook 2012*. 2012.
3. J. R. Petit, J.J., D. Raynaud, N. I. Barkov, J.-M. Barnola, I. Basile, M. Bender, J. Chappellaz, M. Davis, G. Delaygue, M. Delmotte, V. M. Kotlyakov, M. Legrand, V. Y. Lipenkov, C. Lorius, L. Pépin, C. Ritz, E. Saltzman M. Stievenard, *Climate and atmospheric history of the past 420,000 years from the Vostok ice core, Antarctica*. Nature, 1999. **399**: p. 429-436.
4. J. M. Barnola, D.R., Y. S. Korotkevich, C. Lorius, *Vostok ice core provides 160,000-year record of atmospheric CO₂*. Nature, 1987. **329**: p. 408-414.
5. Keeling, C.D.a.T.P.W. *Atmospheric CO₂ Records from Sites in the SIO Air Sampling Network*. 2004; Available from: <http://cdiac.ornl.gov/trends/co2/sio-keel.html>.
6. Neftel, A., E. Moor, H. Oeschger, and B. Stauffer, *Evidence from polar ice cores for the increase in atmospheric CO₂ in the past two centuries*. Nature, 1985. **311**(45-47).
7. United-Nations. *Kyoto Protocol*. Available from: http://unfccc.int/essential_background/kyoto_protocol/items/6034.php.
8. Martin I. Hoffert, K.C., Atul K. Jain, Erik F. Haites, L. D. Danny Harveyk, Seth D. Potter, Michael E. Schlesinger, Stephen H. Schneider, Robert G. Watts, Tom M. L. Wigley**& Donald J. Wuebbles, *Energy implications of future stabilization of atmospheric CO₂ content*. Nature, 395. **395**(6705): p. 881-884.
9. N.S. Lewis, G.W.C., *Basic Research needs for Solar Energy Utilization: report of the basic energy workshop on solar energy utilization, April 18-21, 2005*. US Department of energy office of basic energy sciences, 2005.
10. eia, *ANNUAL ENERGY OUTLOOK 2012*. July 2012.
11. Shockley, W. and H.J. Queisser, *Detailed Balance Limit of Efficiency of p-n Junction Solar Cells*. Journal of Applied Physics, 1961. **32**(3): p. 510-519.
12. Green, M.A., et al., *Solar cell efficiency tables (version 39)*. Progress in Photovoltaics: Research and Applications, 2012. **20**(1): p. 12-20.
13. R. McNeil, R.S., J.H. Wardlaw, D.E. Weiss, *Electronic conduction in polymers I. the chemical structure of polypyrrole*. Australian Journal of Chemistry, 1963(16): p. 1056-1075.
14. Shirakawa, H., et al., *Synthesis of electrically conducting organic polymers: halogen derivatives of polyacetylene, (CH)*. Journal of the Chemical Society, Chemical Communications, 1977(16): p. 578-580.
15. Nobelprize.org. *The Nobel Prize in Chemistry 2000*. 2 dec 2000; Available from: http://www.nobelprize.org/nobel_prizes/chemistry/laureates/2000/.

16. Burroughes, J.H., et al., *Light-emitting diodes based on conjugated polymers*. Nature, 1990. **347**(6293): p. 539-541.
17. Yang, Y. and A.J. Heeger, *A NEW ARCHITECTURE FOR POLYMER TRANSISTORS*. Nature, 1994. **372**(6504): p. 344-346.
18. Søndergaard, R.R., M. Hösel, and F.C. Krebs, *Roll-to-Roll fabrication of large area functional organic materials*. Journal of Polymer Science Part B: Polymer Physics. **51**(1): p. 16-34.
19. Letian Dou, J.Y., Jun Yang, Chun-Chao Chen, Youjun He, Seiichiro Murase, Tom Moriarty, Keith Emery, Gang Li & Yang Yang, *Tandem polymer solar cells featuring a spectrally matched low-bandgap polymer*. Nature Photonics, 2012. **6**(3): p. 180-185.
20. *Heliatek sets new world record efficiency of 10.7 % for its organic tandem cell*. July 24, 2012; Available from: http://www.heliatek.com/newscenter/latest_news/heliatek-erzielt-mit-107-effizienz-neuen-weltrekord-fur-seine-organische-tandemzelle/?lang=en#.
21. Tipnis, R., et al., *Large-area organic photovoltaic module—Fabrication and performance*. Solar Energy Materials and Solar Cells, 2009. **93**(4): p. 442-446.
22. Jin, H., et al., *Efficient, Large Area ITO-and-PEDOT-free Organic Solar Cell Sub-modules*. Advanced Materials, 2012. **24**(19): p. 2572-2577.
23. Jørgensen, M., K. Norrman, and F.C. Krebs, *Stability/degradation of polymer solar cells*. Solar Energy Materials and Solar Cells, 2008. **92**(7): p. 686-714.
24. Leif A. A. Pettersson, L.S.R., and Olle Inganäs, *Modeling photocurrent action spectra of photovoltaic devices based on organic thin films*. Journal of applied physics, 1999. **86**(1): p. 487-496.
25. J. J. M. Halls, K.P., R. H. Friend, S. C. Moratti, and A. B. Holmes, *Exciton diffusion and dissociation in a poly(p-phenylenevinylene)/C60 heterojunction photovoltaic cell*. Journal of Applied Physics, 1996. **68**(22): p. 3120-3122.
26. Tang, C.W., *Two-layer organic photovoltaic cell*. Applied Physics Letters, 1986. **48**(2): p. 183-185.
27. Hummelen, J.C., et al., *Preparation and Characterization of Fulleroid and Methanofullerene Derivatives*. The Journal of Organic Chemistry, 1995. **60**(3): p. 532-538.
28. Sariciftci, N.S., et al., *Photoinduced Electron Transfer from a Conducting Polymer to Buckminsterfullerene*. Science, 1992. **258**(5087): p. 1474-1476.
29. Huynh, W.U., J.J. Dittmer, and A.P. Alivisatos, *Hybrid Nanorod-Polymer Solar Cells*. Science, 2002. **295**(5564): p. 2425-2427.
30. Wang, P., et al., *Photoinduced Charge Transfer and Efficient Solar Energy Conversion in a Blend of a Red Polyfluorene Copolymer with CdSe Nanoparticles*. Nano Letters, 2006. **6**(8): p. 1789-1793.

31. J. J. M. Halls, C.A.W., N. C. Greenham, E. A. Marseglia, R. H. Friend, S. C. Moratti & A. B. Holmes, *Efficient photodiodes from interpenetrating polymer networks*. Nature, 1995. **376**: p. 498-500.
32. McNeill, C.R., *Morphology of all-polymer solar cells*. Energy & Environmental Science, 2012. **5**(2): p. 5653-5667.
33. Westenhoff, S., et al., *Charge Recombination in Organic Photovoltaic Devices with High Open-Circuit Voltages*. Journal of the American Chemical Society, 2008. **130**(41): p. 13653-13658.
34. Köhler, A. and D. Beljonne, *The singlet-Triplet Exchange Energy in Conjugated Polymers*. Advanced Functional Materials, 2004. **14**(1): p. 11-18.
35. Veldman, D., S.C.J. Meskers, and R.A.J. Janssen, *The Energy of Charge-Transfer States in Electron Donor–Acceptor Blends: Insight into the Energy Losses in Organic Solar Cells*. Advanced Functional Materials, 2009. **19**(12): p. 1939-1948.
36. Shoaee, S., et al., *Acceptor Energy Level Control of Charge Photogeneration in Organic Donor/Acceptor Blends*. Journal of the American Chemical Society, 2010. **132**(37): p. 12919-12926.
37. Clarke, T.M., et al., *Analysis of Charge Photogeneration as a Key Determinant of Photocurrent Density in Polymer: Fullerene Solar Cells*. Advanced Materials, 2010. **22**(46): p. 5287-5291.
38. Clarke, T., et al., *Transient absorption spectroscopy of charge photogeneration yields and lifetimes in a low bandgap polymer/fullerenefilm*. Chemical Communications, 2009(1): p. 89-91.
39. Dimitrov, S.D., et al., *On the Energetic Dependence of Charge Separation in Low-Band-Gap Polymer/Fullerene Blends*. Journal of the American Chemical Society, 2012. **134**(44): p. 18189-18192.
40. Vandewal, K., et al., *The Relation Between Open-Circuit Voltage and the Onset of Photocurrent Generation by Charge-Transfer Absorption in Polymer : Fullerene Bulk Heterojunction Solar Cells*. Advanced Functional Materials, 2008. **18**(14): p. 2064-2070.
41. Panda, P., et al., *Charge Transfer Absorption for π -Conjugated Polymers and Oligomers Mixed with Electron Acceptors*. The Journal of Physical Chemistry B, 2007. **111**(19): p. 5076-5081.
42. Sariciftci, N.S., et al., *Semiconducting polymer-buckminsterfullerene heterojunctions: Diodes, photodiodes, and photovoltaic cells*. Applied Physics Letters, 1993. **62**(6): p. 585-587.
43. Yu, G., et al., *Polymer Photovoltaic Cells: Enhanced Efficiencies via a Network of Internal Donor-Acceptor Heterojunctions*. Science, 1995. **270**(5243): p. 1789-1791.
44. Collins, B.A., et al., *Molecular Miscibility of Polymer–Fullerene Blends*. The Journal of Physical Chemistry Letters, 2010. **1**(21): p. 3160-3166.

45. Walheim, S., et al., *Structure Formation via Polymer Demixing in Spin-Cast Films*. *Macromolecules*, 1997. **30**(17): p. 4995-5003.
46. Ho, P.K.H., et al., *Solvent Effects on Chain Orientation and Interchain π -Interaction in Conjugated Polymer Thin Films: Direct Measurements of the Air and Substrate Interfaces by Near-Edge X-ray Absorption Spectroscopy*. *Advanced Materials*, 2007. **19**(2): p. 215-221.
47. Nilsson, S., et al., *Morphology and Phase Segregation of Spin-Casted Films of Polyfluorene/PCBM Blends*. *Macromolecules*, 2007. **40**(23): p. 8291-8301.
48. Müller, C., et al., *Influence of Molecular Weight on the Performance of Organic Solar Cells Based on a Fluorene Derivative*. *Advanced Functional Materials*, 2010. **20**(13): p. 2124-2131.
49. Peet, J., et al., *Efficiency enhancement in low-bandgap polymer solar cells by processing with alkane dithiols*. *Nature Materials*, 2007. **6**(7): p. 497-500.
50. Lee, J.K., et al., *Processing Additives for Improved Efficiency from Bulk Heterojunction Solar Cells*. *Journal of the American Chemical Society*, 2008. **130**(11): p. 3619-3623.
51. Hoven, C.V., et al., *Improved Performance of Polymer Bulk Heterojunction Solar Cells Through the Reduction of Phase Separation via Solvent Additives*. *Advanced Materials*, 2010. **22**(8): p. E63-E66.
52. He, M., F. Qiu, and Z. Lin, *Conjugated rod-coil and rod-rod block copolymers for photovoltaic applications*. *Journal of Materials Chemistry*, 2012. **21**(43): p. 17039-17048.
53. Kugler, T., et al., *Polymer band alignment at the interface with indium tin oxide: consequences for light emitting devices*. *Chemical Physics Letters*, 1999. **310**(5-6): p. 391-396.
54. Hoffmann, R., C. Janiak, and C. Kollmar, *A chemical approach to the orbitals of organic polymers*. *Macromolecules*, 1991. **24**(13): p. 3725-3746.
55. Wudl, F., M. Kobayashi, and A.J. Heeger, *Poly(isothianaphthene)*. *The Journal of Organic Chemistry*, 1984. **49**(18): p. 3382-3384.
56. Liang, Y., et al., *Development of New Semiconducting Polymers for High Performance Solar Cells*. *Journal of the American Chemical Society*, 2008. **131**(1): p. 56-57.
57. Havinga, E.E., W. Hovee, and H. Wynberg, *A new class of small band gap organic polymer conductors*. *Polymer Bulletin*, 1992. **29**(1-2): p. 119-126.
58. Steyrleuthner, R., et al., *Aggregation in a High-Mobility n-Type Low-Bandgap Copolymer with Implications on Semicrystalline Morphology*. *Journal of the American Chemical Society*, 2012. **134**(44): p. 18303-18317.
59. Köhler, A., S.T. Hoffmann, and H. Bässler, *An Order-Disorder Transition in the Conjugated Polymer MEH-PPV*. *Journal of the American Chemical Society*, 2012. **134**(28): p. 11594-11601.

60. Svensson, M., et al., *High-Performance Polymer Solar Cells of an Alternating Polyfluorene Copolymer and a Fullerene Derivative*. *Advanced Materials*, 2003. **15**(12): p. 988-991.
61. Wang, E., et al., *High-performance polymer heterojunction solar cells of a polysilafluorene derivative*. *Applied Physics Letters*, 2008. **92**(3): p. 033307-3.
62. Blouin, N., A. Michaud, and M. Leclerc, *A Low-Bandgap Poly(2,7-Carbazole) Derivative for Use in High-Performance Solar Cells*. *Advanced Materials*, 2007. **19**(17): p. 2295-2300.
63. McCulloch, I., et al., *Design of Semiconducting Indacenodithiophene Polymers for High Performance Transistors and Solar Cells*. *Accounts of Chemical Research*. **45**(5): p. 714-722.
64. Schwarz, C., et al., *Does Conjugation Help Exciton Dissociation? A Study on Poly(p-phenylene)s in Planar Heterojunctions with C60 or TNF*. *Advanced Materials*, 2012. **24**(7): p. 922-925.
65. Hess, B.A. and L.J. Schaad, *Hueckel molecular orbital .pi.-resonance energies. Heterocycles containing divalent sulfur*. *Journal of the American Chemical Society*, 1973. **95**(12): p. 3907-3912.
66. Mintmire, J.W., C.T. White, and M.L. Elert, *Conformation and electronic structure of heterocyclic ring chain polymers*. *Synthetic Metals*, 1988. **25**(2): p. 109-119.
67. Kroon, R., et al., *Effect of electron-withdrawing side chain modifications on the optical properties of thiophene-quinoxaline acceptor based polymers*. *Polymer*, 2013(0).
68. Mayer, A.C., et al., *Bimolecular Crystals of Fullerenes in Conjugated Polymers and the Implications of Molecular Mixing for Solar Cells*. *Advanced Functional Materials*, 2009. **19**(8): p. 1173-1179.
69. Zhang, X., et al., *Molecular Packing of High-Mobility Diketo Pyrrolo-Pyrrole Polymer Semiconductors with Branched Alkyl Side Chains*. *Journal of the American Chemical Society*, 2011. **133**(38): p. 15073-15084.
70. Ko, S., et al., *Controlled Conjugated Backbone Twisting for an Increased Open-Circuit Voltage while Having a High Short-Circuit Current in Poly(hexylthiophene) Derivatives*. *Journal of the American Chemical Society*, 2012. **134**(11): p. 5222-5232.
71. Chen, T.A. and R.D. Rieke, *The first regioregular head-to-tail poly(3-hexylthiophene-2,5-diyl) and a regiorandom isopolymer: nickel versus palladium catalysis of 2(5)-bromo-5(2)-(bromozincio)-3-hexylthiophene polymerization*. *Journal of the American Chemical Society*, 1992. **114**(25): p. 10087-10088.
72. Kawahara, H., et al., *Third-order optical nonlinearity in regioregular head-to-tail coupled poly(3-Hexylthiophene)*. *Optical Review*, 1997. **4**(1): p. 188-190.
73. Brinkmann, M. and P. Rannou, *Effect of Molecular Weight on the Structure and Morphology of Oriented Thin Films of Regioregular Poly(3-hexylthiophene) Grown by Directional Epitaxial Solidification*. *Advanced Functional Materials*, 2007. **17**(1): p. 101-108.

74. Padinger, F., R.S. Rittberger, and N.S. Sariciftci, *Effects of Postproduction Treatment on Plastic Solar Cells*. *Advanced Functional Materials*, 2003. **13**(1): p. 85-88.
75. Boudreault, P.-L.T., A. Michaud, and M. Leclerc, *A New Poly(2,7-Dibenzosilole) Derivative in Polymer Solar Cells*. *Macromolecular Rapid Communications*, 2007. **28**(22): p. 2176-2179.
76. Usta, H., et al., *Dithienosilole- and Dibenzosilole-Thiophene Copolymers as Semiconductors for Organic Thin-Film Transistors*. *Journal of the American Chemical Society*, 2006. **128**(28): p. 9034-9035.
77. Yamaguchi, S. and K. Tamao, *Silole-containing [sigma]- and [small pi]-conjugated compounds*. *Journal of the Chemical Society, Dalton Transactions*, 1998. **0**(22): p. 3693-3702.
78. Chan, K.L., et al., *Poly(2,7-dibenzosilole): A Blue Light Emitting Polymer*. *Journal of the American Chemical Society*, 2005. **127**(21): p. 7662-7663.
79. Manceau, M., et al., *Photochemical stability of [small pi]-conjugated polymers for polymer solar cells: a rule of thumb*. *Journal of Materials Chemistry*, 2011. **21**(12): p. 4132-4141.
80. Chen, H.-Y., et al., *Silicon Atom Substitution Enhances Interchain Packing in a Thiophene-Based Polymer System*. *Advanced Materials*, 2010. **22**(3): p. 371-375.
81. Scharber, M.C., et al., *Influence of the Bridging Atom on the Performance of a Low-Bandgap Bulk Heterojunction Solar Cell*. *Advanced Materials*, 2010. **22**(3): p. 367-370.
82. Robert C. Coffin, J.P., James Rogers, Guillermo C. Bazan, *Streamlined microwave-assisted preparation of narrow-bandgap conjugated polymers for high-performance bulk heterojunction solar cells*. *Nature Chemistry*, 2009. **1**: p. 657-661.
83. Zhang, F., et al., *High photovoltage achieved in low band gap polymer solar cells by adjusting energy levels of a polymer with the LUMOs of fullerene derivatives*. *Journal of Materials Chemistry*, 2008. **18**(45): p. 5468-5474.
84. Lindgren, L.J., et al., *Synthesis, Characterization, and Devices of a Series of Alternating Copolymers for Solar Cells*. *Chemistry of Materials*, 2009. **21**(15): p. 3491-3502.
85. Scharber, M.C., et al., *Influence of the Bridging Atom on the Performance of a Low-Bandgap Bulk Heterojunction Solar Cell*. *Advanced Materials*, 2009. **22**(3): p. 367-370.
86. Rieger, R., et al., *Backbone Curvature in Polythiophenes*. *Chemistry of Materials*, 2010. **22**(18): p. 5314-5318.
87. Yamamoto, T., et al., *Synthesis of a New Thiophene/Quinoxaline CT-Type Copolymer with High Solubility and Its Basic Optical Properties*. *Macromolecular Rapid Communications*, 2003. **24**(7): p. 440-443.
88. Wang, E., et al., *An Easily Synthesized Blue Polymer for High-Performance Polymer Solar Cells*. *Advanced Materials*, 2010. **22**(46): p. 5240-5244.

89. Espinet, P. and A.M. Echavarren, *The Mechanisms of the Stille Reaction*. Angewandte Chemie International Edition, 2004. **43**(36): p. 4704-4734.
90. Laiho, A., et al., *Control of Self-Assembly by Charge-Transfer Complexation between C60 Fullerene and Electron Donating Units of Block Copolymers*. Macromolecules, 2006. **39**(22): p. 7648-7653.
91. Lehnert, W., *Verbesserte variante der knoevenagel-kondensation mit TiCl4/THF/pyridin(I). Alkyliden- und Arylidenmalonester bei 0-25Å°C*. Tetrahedron Letters, 1970. **11**(54): p. 4723-4724.
92. Moet, D.J.D., et al., *Impact of molecular weight on charge carrier dissociation in solar cells from a polyfluorene derivative*. Organic Electronics, 2009. **10**(7): p. 1275-1281.
93. Schilinsky, P., et al., *Influence of the Molecular Weight of Poly(3-hexylthiophene) on the Performance of Bulk Heterojunction Solar Cells*. Chemistry of Materials, 2005. **17**(8): p. 2175-2180.
94. Pan, H., et al., *Benzodithiophene Copolymer—A Low-Temperature, Solution-Processed High-Performance Semiconductor for Thin-Film Transistors*. Advanced Functional Materials, 2007. **17**(17): p. 3574-3579.
95. Price, S.C., et al., *Fluorine Substituted Conjugated Polymer of Medium Band Gap Yields 7% Efficiency in Polymer–Fullerene Solar Cells*. Journal of the American Chemical Society, 2011. **133**(12): p. 4625-4631.
96. Tanimoto, A. and T. Yamamoto, *Synthesis of n-Type Poly(benzotriazole)s Having p-Conducting and Polymerizable Carbazole Pendants*. Macromolecules, 2006. **39**(10): p. 3546-3552.
97. Hou, L., et al., *Lateral Phase Separation Gradients in Spin-Coated Thin Films of High-Performance Polymer:Fullerene Photovoltaic Blends*. Advanced Functional Materials, 2011. **21**(16): p. 3169-3175.
98. Tromholt, T., et al., *Photochemical stability of conjugated polymers, electron acceptors and blends for polymer solar cells resolved in terms of film thickness and absorbance*. Journal of Materials Chemistry, 2012. **22**(15): p. 7592-7601.
99. Hao, Z. and A. Iqbal, *Some aspects of organic pigments*. Chemical Society Reviews, 1997. **26**(3): p. 203-213.
100. J. Mizuguchi, A.G., G. Wooden and G. Rihs, *Structures of 3,6-diphenylpyrrolo[3,4-c]pyrrole-1,4-dione and 2,5-dimethyl-3,6-diphenylpyrrolo[3,4-c]pyrrole-1,4-dione*. Acta Crystalligraphica, 1992. **B48**: p. 696-700.
101. Bronstein, H., et al., *Thieno[3,2-b]thiophene-Diketopyrrolopyrrole-Containing Polymers for High-Performance Organic Field-Effect Transistors and Organic Photovoltaic Devices*. Journal of the American Chemical Society, 2011. **133**(10): p. 3272-3275.

102. Bijleveld, J.C., et al., *Efficient Solar Cells Based on an Easily Accessible Diketopyrrolopyrrole Polymer*. *Advanced Materials*, 2010. **22**(35): p. E242-E246.

